

*Department of Construction Sciences*  
Solid Mechanics

ISRN LUTFD2/TFHF-10/5153-SE(1-56)

# A TOPOLOGY OPTIMIZATION METHOD BASED ON THE CAHN-HILLIARD MODEL

Master Thesis by  
HENRIK ASKFELT

SUPERVISOR  
DOCENT MATHIAS WALLIN, DIV. OF SOLID MECHANICS

EXAMINER  
PROF. MATTI RISTINMAA, DIV. OF SOLID MECHANICS

Copyright © 2010 by Div. of Solid Mechanics and Henrik Askfelt  
Printed by Media-Tryck, Lund, Sweden

For information, address:  
Division of Solid Mechanics, Lund University, Box 118, SE-221 00 Lund, Sweden.  
Homepage: <http://www.solid.lth.se>



## Abstract

Structural optimization is a rather new branch in solid mechanics that have become increasingly important during the last decades.

The SIMP method is a simple and fast method frequently used to obtain optimized structures. The SIMP method has in a finite element setting a well known defect in that it lacks a unique solution which appears as a mesh dependency.

To circumvent this mesh dependency a structural optimization method allowing for perimeter control is presented. The procedure is based on a functional in terms of the material density distribution and the displacement field. The optimum of the functional is found by using the KKT conditions and Cahn-Hilliards equation. To solve the problem use is made of the finite element method. To properly resolve the interfaces of the optimized structure an adaptive space discretization is implemented.

To test the method and verify that the formulation returns feasible structures, simulations are performed on a simple optimization problem. The results from these simulations are reasonable and we conclude that the method is working for the simple optimization problems that are tested.

# Contents

<b>1</b>	<b>Introduction</b>	<b>2</b>
1.1	Introduction . . . . .	3
1.1.1	Example . . . . .	4
1.2	Finite element formulation of two-dimensional elasticity . . . . .	7
1.3	Minimizing the compliance . . . . .	9
<b>2</b>	<b>Part A</b>	<b>11</b>
2.1	Topology-Optimization using SIMP . . . . .	11
2.1.1	Convex Problem . . . . .	12
2.1.2	Convex approximation . . . . .	14
2.1.3	Calculating the optimal construction . . . . .	17
2.1.4	Results from using the SIMP method . . . . .	20
<b>3</b>	<b>Part B</b>	<b>23</b>
3.1	Topology optimization based on Cahn-Hilliard equation . . . . .	23
3.1.1	Defining the optimization problem $\mathcal{P}^B$ . . . . .	23
3.1.2	Deriving the stationarity point . . . . .	28
3.1.3	Cahn-Hilliards Equation Three node elements . . . . .	31
3.1.4	Finite element formulation . . . . .	33
3.1.5	Three-Node Triangles . . . . .	35
3.1.6	Newton Raphson . . . . .	40
3.1.7	Adaptive Mesh . . . . .	41
3.1.8	Results from Part B . . . . .	46
3.2	Appendix1 . . . . .	56
3.2.1	The matrices in equations (1.11) - (1.13) . . . . .	56
3.2.2	Derivatives of $\tilde{f}_i$ . . . . .	56
3.2.3	Derivatives of $\tilde{g}$ . . . . .	56

# Chapter 1

## Introduction

## 1.1 Introduction

Many processes when constructing new products can be modeled as schemes similar to the one illustrated in Figure 1.1.

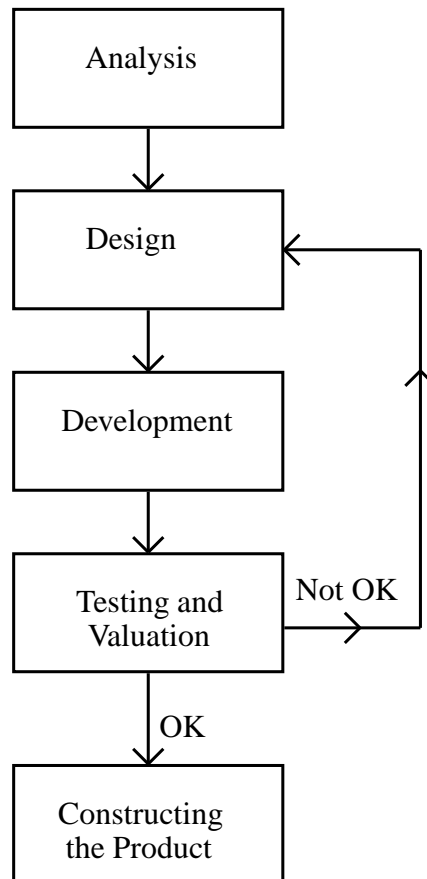


Figure 1.1: Model of a product development

To get a better understanding of this process each step is described beneath

- 1 Analysis:** In this step an analyze is made regarding what demands the product needs to fulfill and what the limitations for constructing it might be.
- 2 Design:** At this step a guess is made on how the product should be constructed. Here it is almost always preferable to use engineers that have had a lot of experience with similar products before since they make the best guesses.

**3 Development:** The construction following the *Design step* is not perfect and therefore improvements are performed in this step.

**4 Testing and Valuation:** The product is tested to confirm that it fulfills the demands specified in the *Analysis step* and also if it does so in the best possible way. At this point it is common to realize that the product still needs improvement and if this is the case a "jump" is made back to the *Design step*. When this cycle has been performed a couple of times or, which sometimes is the case, a lot of times one will hopefully be satisfied with the product and move on to the last step.

**5 Constructing the product:** This is when the product is constructed

The process of performing these 5 steps is very time consuming and therefore also consumes a lot of money. These issues of time and money are two of the main reasons why structural optimization theory have become increasingly important during the last decades. The theory behind structural optimization is a rather new branch in solid mechanics but has already delivered models that in many cases can advance the product development better than the model described by Figure 1.1. Some of these models still have room for improvement and this is what motivated this thesis.

### 1.1.1 Example

To show the effect of an optimization, while simultaneously describing different models of performing an optimization, a simple example is given.

**Example 1:**

Assume that there lies a need of a structure that can withstand an external force  $P$ . Assume also that the amount of material available for the construction is limited and that the structure is to be placed within the area  $A$ . For clarity the problem is illustrated in Figure 1.2.

The need for a structure that can withstand an external force  $P$  motivates the search of a structure that is as stiff as possible. Maximizing the stiffness of the structure is equivalent to minimizing the compliance of the structure. Since minimizing the compliance is an easier problem to handle the compliance is going to be used as an objective of the optimization.

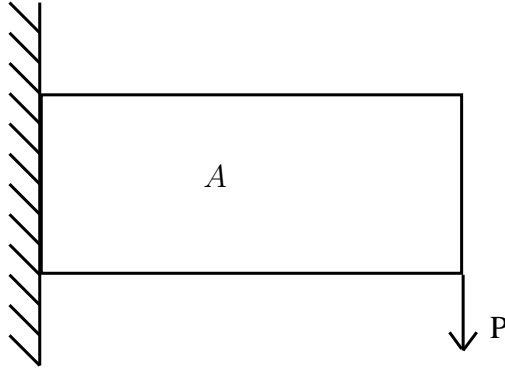


Figure 1.2: Illustration of the customers demands

To performing this optimization it is convenient to define an objective function  $g_0 = C$  where  $C$  denotes the compliance and then minimize  $g_0$ . Since the structure is limited by the amount of material available a volume constraint  $g_1$  must be imposed to the optimization.

When dealing with optimization problems it is found useful to rewrite the problem into a mathematical problem. Let  $\mathcal{P}$  denote a *general* mathematical optimization problem and define it by:

$$\mathcal{P} = \begin{cases} \min_{\boldsymbol{\rho} \in \mathbb{R}^m} g_0(\boldsymbol{\rho}, \mathbf{u}) \\ s.t \begin{cases} \sigma_{kl,l} + b_k = 0 \\ g_i \leq 0 \text{ for } i = 1 \dots n \\ \rho_e \in \chi = \{\rho_e \in \mathbb{R}^m : \rho_e^{min} \leq \rho_e \leq \rho_e^{max}\} \end{cases} \end{cases} \quad (1.1)$$

where  $\mathbf{u}$  denotes the displacement vector,  $g_i$  denotes the constraints and  $\rho_e \in \chi$  is called a box constraint. When solving  $\mathcal{P}$  use will be made of the finite element method which means that the structure is discretized into a number of elements  $e$ . The concentration  $\rho_e$  is for each of these elements element  $e$  assumed to be constant over the whole element. Due to the manufacturing process it is in many cases desirable to end up with a distinct design i.e.  $\rho_e \in \{0, 1\} \forall e$ , where  $\rho_e = 1$  means there is material and  $\rho_e = 0$  means no material. Furthermore is the equilibrium equation  $\sigma_{kl,l} + b_k = 0$  included in (1.1) to impose that the local form of the static equilibrium is to be fulfilled. Here is  $\sigma_{kl}$  the Cauchy stress tensor and  $b_k$  the body force vector.

In Part A of this thesis the SIMP method is discussed. This method takes the three demands in **Example 1** in mind. However, it is well known that the SIMP method results in a mesh dependent solution and therefore does not have a unique solution.

In Part B another method based on adding two penalization functions is derived. The resulting equations will be solved using the Cahn-Hilliard equation and the space-discretization is based on an adaptive three node mesh.

Before these Parts are presented two sections are included describing the *finite element formulation of the two dimensional elasticity* and some properties regarding *minimization of the compliance*

## 1.2 Finite element formulation of two-dimensional elasticity

Let the local form of the static equilibrium define the strong form of elasticity as

$$\sigma_{ij,j} + b_i = 0 \quad (1.2)$$

Multiplying equation (1.2) with a weight function  $\bar{v}_l$  and integrating over the domain  $\Omega$  gives

$$\int_{\Omega} \bar{v}_l \sigma_{ij,j} d\Omega + \int_{\Omega} \bar{v}_l b_i d\Omega = 0. \quad (1.3)$$

Applying the product rule

$$\bar{v}_l \sigma_{ij,j} = (\bar{v}_l \sigma_{ij})_{,j} - \bar{v}_{l,j} \sigma_{ij} \quad (1.4)$$

to substitute the term  $\bar{v}_l \sigma_{ij,j}$  results in

$$\int_{\Omega} (\bar{v}_l \sigma_{ij})_{,j} d\Omega - \int_{\Omega} \bar{v}_{l,j} \sigma_{ij} d\Omega + \int_{\Omega} \bar{v}_l b_i d\Omega = 0 \quad (1.5)$$

Which after making use of *divergence theorem of Gauss*

$$\int_V q_{i,i} dV = \int_S q_i n_i dS. \quad (1.6)$$

to equation (1.5) the weak form of elasticity follows

$$\int_{\partial\Omega} \bar{v}_l t_i d\partial\Omega - \int_{\Omega} \bar{v}_{l,j} \sigma_{ij} d\Omega + \int_{\Omega} \bar{v}_l b_i d\Omega = 0. \quad (1.7)$$

In equation (1.7) use have been made of Cauchy's formula which states

$$t_i = \sigma_{ij} n_j \quad (1.8)$$

where  $t_i$  denotes the traction vector.

Inserting the following FE-approximations

$$\mathbf{u} = \mathbf{N}_m \bar{\mathbf{u}} \quad \boldsymbol{\varepsilon} = \mathbf{B}_m \bar{\mathbf{u}} \quad (1.9)$$

$$\bar{v}_l = \mathbf{N}_m \bar{\mathbf{v}} \quad \bar{v}_{l,j} = \mathbf{B}_m \bar{\mathbf{v}} \quad (1.10)$$

into the weak form (1.7) defines the finite element formulation of the two-dimensional elasticity as

$$\mathbf{K}\mathbf{u} = \mathbf{P} \quad (1.11)$$

$$\mathbf{K} = \int_{\Omega} \mathbf{B}_m^T \mathbf{D} \mathbf{B}_m d\Omega \quad (1.12)$$

$$\mathbf{P} = \int_{\partial\Omega} \mathbf{N}_m^T \mathbf{t} d\partial\Omega + \int_{\Omega} \mathbf{N}_m^T \mathbf{b} d\Omega \quad (1.13)$$

where  $D$  denotes the element stiffness tensor which here is defined by

$$\mathbf{D} = \tilde{f} \mathbf{D}^0 \quad (1.14)$$

Here  $\tilde{f}$  is a function of the local concentration  $\rho_e$  and  $\mathbf{D}^0$  is the stiffness tensor defined by hookes law i.e.

$$\tilde{f} = \tilde{f}(\rho_e) \quad (1.15)$$

$$\mathbf{D}^0 = \frac{E}{1-\nu^2} \begin{pmatrix} 1 & \nu & 0 \\ \nu & 1 & 0 \\ 0 & 0 & \frac{1-\nu}{2} \end{pmatrix}. \quad (1.16)$$

Different choices of  $\tilde{f}$  will be discussed in this thesis. Note that this definition of the stiffness tensor allow the global stiffness matrix  $\mathbf{K}(\boldsymbol{\rho})$  to be separated as

$$\mathbf{K}(\boldsymbol{\rho}) = \sum_{e=1}^n \tilde{f}(\rho_e) \mathbf{K}_e^0 \quad (1.17)$$

Making use of equation (1.11) the mathematical problem  $\mathcal{P}$  is rewritten into

$$\mathcal{P} = \begin{cases} \min_{\boldsymbol{\rho} \in \mathbb{R}^m} g_0(\boldsymbol{\rho}, \mathbf{u}) \\ \text{s.t.} \begin{cases} \mathbf{K}(\boldsymbol{\rho}) \mathbf{u}(\boldsymbol{\rho}) = \mathbf{P} \\ g_i \leq 0 \text{ for } i = 1 \dots n \\ \rho_e \in \chi \end{cases} \end{cases} \quad (1.18)$$

cf. (1.1)

The matrices in equations (1.11) - (1.13) are defined in Section 3.2

### 1.3 Minimizing the compliance

To simplify the derivation of the optimization methods this section will present some properties associated with optimization of the compliance.

The compliance is defined as

$$C = \int_{\partial\Omega} t_i u_i d\partial\Omega + \int_{\Omega} b_i u_i d\Omega. \quad (1.19)$$

Using the compliance as an objective function results in a problem that contains the two design parameters  $u_i$  and  $\rho_e$ . These variables are coupled via equilibrium which is a property that can be eluded through

$$\mathbf{u}(\boldsymbol{\rho}) = \mathbf{K}^{-1}(\boldsymbol{\rho})\mathbf{P}. \quad (1.20)$$

cf. (1.11)

Using the coupling (1.20) the nested mathematical problem  $\mathcal{P}_{nf}$  originated from  $\mathcal{P}$  is obtained.  $\mathcal{P}_{nf}$  is defined as

$$\mathcal{P}_{nf} = \begin{cases} \min_{\boldsymbol{\rho} \in \mathbb{R}^m} g_0(\boldsymbol{\rho}) \\ \text{s.t.} \begin{cases} g_i \leq 0 \text{ for } i = 1 \dots n \\ \rho_e \in \chi = \{\rho_e \in \mathbb{R}^m : \rho^{min} \leq \rho_e \leq \rho^{max}\} \end{cases} \end{cases} \quad (1.21)$$

Rewriting equation (1.19) with Cauchy's formula (1.8) and the local form of the static equilibrium equations (1.2) results in

$$C = \int_{\partial\Omega} \sigma_{ij} n_j u_i d\partial\Omega - \int_{\Omega} u_i \sigma_{ij,j} d\Omega. \quad (1.22)$$

Which after applying the product rule

$$(u_i \sigma_{ij})_{,j} = u_{i,j} \sigma_{ij} + u_i \sigma_{ij,j} \quad (1.23)$$

and *Gauss theorem* (1.6) enables the second integral in (1.22) to be rewritten as

$$\int_{\Omega} u_i \sigma_{ij,j} d\Omega = \int_{\partial\Omega} u_i \sigma_{ij} n_j d\partial\Omega - \int_{\Omega} u_{i,j} \sigma_{ij} d\Omega \quad (1.24)$$

Since  $\sigma_{ij} = \sigma_{ji}$  the displacement gradient  $u_{i,j}$  can be replaced by the strain tensor  $\varepsilon_{ij}$ . Making this change in equation (1.24) the following is obtained

$$C = \int_{\Omega} \varepsilon_{ij} \sigma_{ij} d\Omega = \int_{\Omega} \varepsilon_{ij} D_{ijkl} \varepsilon_{kl} d\Omega. \quad (1.25)$$

Note that equation (1.25) states that the compliance is proportional to the strain energy integrated over the domain  $\Omega$  since the strain energy  $w$  is defined as

$$w = \frac{1}{2} \varepsilon_{ij} D_{ijkl} \varepsilon_{kl}. \quad (1.26)$$

Inserting the FE-approximations (cf. Section 1.2) into equation (1.25) gives

$$C = \mathbf{u}^T \mathbf{K} \mathbf{u} \quad (1.27)$$

Combining equations (1.11) and (1.27) results in

$$C = \mathbf{P}^T \mathbf{u} \quad (1.28)$$

where use have been made of the fact that  $\mathbf{K}$  is symmetric

To further motivate equation (1.28) consider Figure 1.3 where a beam is being exposed to an external force  $P$ .

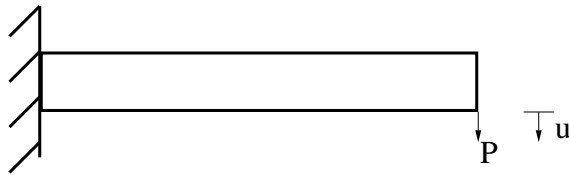


Figure 1.3: Beam exposed to an external force  $P$

From Figure 1.3 one can interpret that a stiff beam would make the deflection  $\mathbf{u}$  smaller than a beam that is not stiff i.e maximizing the stiffness is equivalent with minimizing  $\mathbf{P}^T \mathbf{u}$ .

# Chapter 2

## Part A

### 2.1 Topology-Optimization using SIMP

Solid Isotropic Material with Penalization, SIMP, is a simple and fast method used to obtain an optimized structure. The SIMP-method is based on the optimal criteria method, OC-method, and both these methods are briefly presented so that the reader understands the motivation for this report.

When deriving these methods it is convenient to first present the mathematical problem  $\mathcal{P}$  associated with the two methods cf. (1.21).

Using the compliance as the objective of the optimization the objective function  $g_0$  is for these methods defined by

$$g_0(\boldsymbol{\rho}) = \mathbf{P}^T \mathbf{u}(\boldsymbol{\rho}). \quad (2.1)$$

cf. (1.28)

The volume constraint  $g_1$  that is imposed in the SIMP method is defined by

$$g_1(\boldsymbol{\rho}) = \sum_{e=1}^n a_e \rho_e t_h - V_{max}. \quad (2.2)$$

where  $t_h$  denotes the maximum thickness of the structure, and  $a_e$  the area of element  $e$ . Finally the box constraints which limits the values of the concentration  $\rho_e$  is defined as

$$\rho_e \in \chi = \{\rho_e \in \mathbb{R}^m : \rho_e^{min} \leq \rho_e \leq \rho_e^{max}\} \quad (2.3)$$

$$\text{where } \rho_e^{min} = 4\sqrt{eps} \text{ and } \rho_e^{max} = 1. \quad (2.4)$$

where  $eps$  denotes the machine precision taken as  $eps = 2.2204 \cdot 10^{-16}$ .

Elements where  $\rho_e = \rho_e^{min}$  should be interpreted as elements with no material, the reason why  $\rho_e^{min} \neq 0$  is to avoid singularities.

Inserting equations (2.1)- (2.3) into (1.21) gives

$$\mathcal{P}_{nf}^1 = \begin{cases} \min_{\boldsymbol{\rho}} g_0(\boldsymbol{\rho}) = \mathbf{P}^T \mathbf{u}(\boldsymbol{\rho}) \\ s.t \begin{cases} g_1(\boldsymbol{\rho}) = \sum_e^n a_e \rho_e t_h - V_{max} \leq 0 \\ \rho_e \in \chi = \{\rho_e \in \mathbb{R}^m : \rho_e^{min} \leq \rho_e \leq \rho_e^{max}\} \end{cases} \end{cases} \quad (2.5)$$

To solve problem (2.5) use is being made of convex approximations. To understand the motivation behind this the concept convexity is presented.

### 2.1.1 Convex Problem

A problem is said to be convex if the objective function and all the constraints, including the box constraint, are convex. The definitions of a convex set and a convex function are stated as:

A set  $S \subset \mathbb{R}^n$  is *convex* if for all  $x_1, x_2 \in S$  and all  $\lambda \in [0,1]$ , it holds that

$$\lambda x_1 + (1 - \lambda)x_2 \in S \quad (2.6)$$

Note that this implies that every box constraint on the form  $x_{max} > x > x_{min}$  is a convex set.

A function  $f : S \rightarrow R$  is *convex* if for all  $x_1, x_2 \in S$  with  $x_1 \neq x_2$  and all  $\lambda \in (0,1)$ , it holds that

$$f(\lambda x_1 + (1 - \lambda)x_2) \leq \lambda f(x_1) + (1 - \lambda)f(x_2) \quad (2.7)$$

From these definitions the following lemmas can be shown

- If  $f$  and  $g$  are convex functions, then the sum  $h = f + g$  is also convex
- If  $f$  is on an affine form  $f = ax + b$ , then  $f$  is convex
- If  $f$  is on the form  $f = x^{-\alpha}$  where  $\alpha$  is a positive integer and  $x > 0$ ,  $f$  is convex.
- $f$  is convex on  $I \iff \frac{\partial^2 f}{\partial x^2} \geq 0 \forall x \in I$

What the definitions above means is that a set is convex if all points on a line connecting two points in the set also belongs to the set. A function is convex if the set above the graph of the function is convex. This implies that if a stationarity point is found to a convex function then this is also a global minimum of the function.

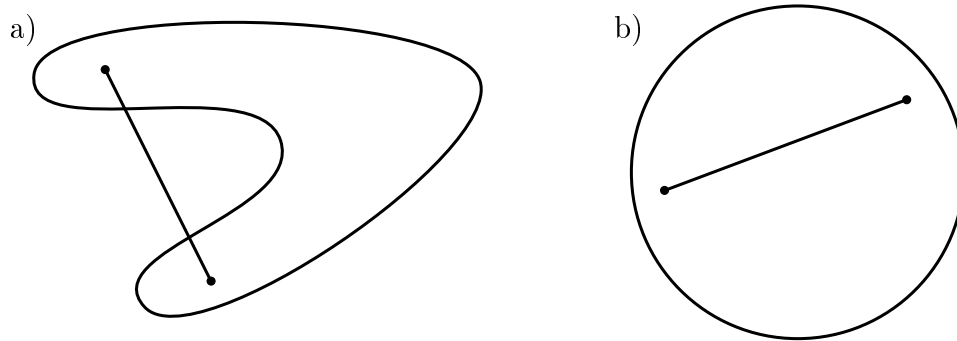


Figure 2.1: Illustrations of a) a set that is not convex b) a set that is convex

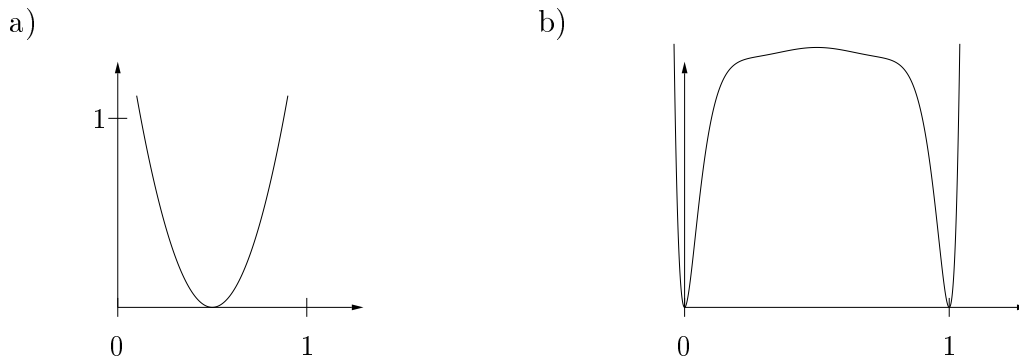


Figure 2.2: Illustrations of a) a function that is convex b) a function that is not convex

## 2.1.2 Convex approximation

### OC-Method

As a first step in deriving the convex approximation  $g^{OC}$  a Taylor expansion of function  $g$  is performed. The Taylor expansion is performed with respect to  $y_e$  which is an intervening variable chosen as

$$y_e = \rho_e^{-\alpha} \quad \alpha \in \mathbf{Z}_+. \quad (2.8)$$

After the Taylor expansion  $g^{OC}$  takes the form

$$g^{OC}(\boldsymbol{\rho}) \approx g(\boldsymbol{\rho}^k) + \sum_{e=1}^n \frac{\partial g(\boldsymbol{\rho})}{\partial y_e} \Big|_{\boldsymbol{\rho}=\boldsymbol{\rho}^k} (y_e - y_e^k) \quad (2.9)$$

where  $\boldsymbol{\rho}^k$  is a known state and

$$\frac{\partial g(\boldsymbol{\rho})}{\partial y_e} = \frac{\partial g(\boldsymbol{\rho})}{\partial \rho_e} \frac{\partial \rho_e}{\partial y_e} = \frac{\partial g(\boldsymbol{\rho})}{\partial \rho_e} \frac{1}{\frac{d(\rho_e^{-\alpha})}{d\rho_e}} = -\frac{\rho_e^{1+\alpha}}{\alpha} \frac{\partial g(\boldsymbol{\rho})}{\partial \rho_e} \quad (2.10)$$

All the functions applied to the OC convex approximation in this thesis will have the following property

$$\frac{\partial g(\boldsymbol{\rho})}{\partial \rho_e} \geq 0. \quad (2.11)$$

Having this property implies that

$$\frac{\partial^2 g^{OC}}{\partial \rho_e^2} \geq 0 \quad \forall \rho_e \in \chi \quad (2.12)$$

which means that  $g^{OC}$  is a convex function cf. Section 2.1.1

Applying the OC convex approximation to the objective function  $g_0$  defined in equation (2.1) the convex approximation  $g_0^{OC}$  is retrieved

$$\frac{\partial g_0(\boldsymbol{\rho})}{\partial \rho_e} = \mathbf{P}^T \frac{\partial \mathbf{u}(\boldsymbol{\rho})}{\partial \rho_e} = (\mathbf{K}(\boldsymbol{\rho}) \mathbf{u}(\boldsymbol{\rho}))^T \frac{\partial \mathbf{u}(\boldsymbol{\rho})}{\partial \rho_e} = \mathbf{u}(\boldsymbol{\rho})^T \mathbf{K}(\boldsymbol{\rho}) \frac{\partial \mathbf{u}(\boldsymbol{\rho})}{\partial \rho_e} \quad (2.13)$$

where use have been made of the fact that  $\mathbf{K}(\boldsymbol{\rho})$  is symmetric and the stiffness tensor is defined by

$$\tilde{f}(\rho_e) = \rho_e \quad (2.14)$$

cf. (1.14).

The derivative of  $\mathbf{K}(\boldsymbol{\rho}) \mathbf{u}(\boldsymbol{\rho}) = \mathbf{P}$  with respect to  $\rho_e$  states

$$\frac{\partial \mathbf{K}(\boldsymbol{\rho})}{\partial \rho_e} \mathbf{u}(\boldsymbol{\rho}) + \mathbf{K}(\boldsymbol{\rho}) \frac{\partial \mathbf{u}(\boldsymbol{\rho})}{\partial \rho_e} = \frac{\partial \mathbf{P}}{\partial \rho_e} = \mathbf{0} \Rightarrow \quad (2.15)$$

$$\frac{\partial \mathbf{u}(\boldsymbol{\rho})}{\partial \rho_e} = -\mathbf{K}^{-1}(\boldsymbol{\rho}) \mathbf{K}_e^0 \mathbf{u}(\boldsymbol{\rho}). \quad (2.16)$$

Inserting (2.16) into (2.13) results in

$$\frac{\partial g_0(\boldsymbol{\rho})}{\partial \rho_e} = -(\mathbf{u}_e^k)^T \mathbf{K}_e^0 \mathbf{u}_e^k. \quad (2.17)$$

Since  $\mathbf{K}_e^0$  is positive definite equation (2.17) implies that

$$\frac{\partial g_0(\boldsymbol{\rho})}{\partial \rho_e} \leq 0. \quad (2.18)$$

Inserting (2.17) into equation (2.9) together with equation (2.10) finally defines the convex approximation of  $g_0$  as

$$g_0^{OC}(\boldsymbol{\rho}) = \xi + \sum_{e=1}^n b_e^k \rho_e^{-\alpha} \quad (2.19)$$

$$\text{where } b_e^k = \frac{1}{\alpha} ((\mathbf{u}_e^k)^T \mathbf{K}_e^0 \mathbf{u}_e^k) (\rho_e^k)^{1+\alpha}. \quad (2.20)$$

where  $\xi = g_0^{OC}(0)$  is constant and of no interest when seeking a minimum to  $g_0^{OC}$ . Since the constraint  $g_1$  is linear an OC-approximation would have no affect, i.e.  $g_1^{OC} = g_1$ .

### SIMP-Method

Performing an optimization with the stiffness tensor defined by equations (1.14) and (2.14) would return a structure where element  $e$  have the thickness  $\rho_e t_h$ ,  $\rho_e \in \{\rho_e^{min} \leq \rho_e \leq \rho_e^{max}\}$  cf. (2.5). This means that a structure with intermediate concentrations is retrieved and such a structure might be difficult to construct. One way to elude this problem is to introduce a penalization for intermediate concentrations. This is easily done by changing  $\tilde{f}(\rho_e)$  from  $\tilde{f}(\rho_e) = \rho_e$  to  $\tilde{f}(\rho_e) = \rho_e^q$  where  $q \in \mathbf{N}_+$ . This change will effect the stiffness of each element and can be interpreted as changing Young's modulus from  $E$  to  $\rho_e^q E$ . The effect of changing Young's modulus is illustrated in Figure 2.3. In this figure it is seen that the concentrations  $\rho_e = 1$  and  $\rho_e = 0$  give a one to one relation with the stiffness while the concentrations  $0 < \rho_e < 1$  does not stiffen the structure as much as they would if  $q = 1$ . Note that

this penalization has the disadvantage of making the the continuous problem  $\mathcal{P}_{nf}^1$  non unique. From a practical point of view this disadvantage appears as a mesh dependency where a finer mesh implies thinner members in the structure.

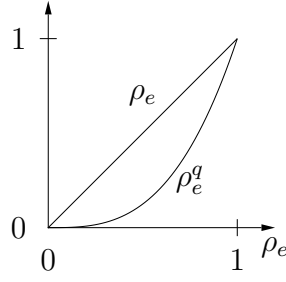


Figure 2.3: Influence of the inserted penalization term  $\rho_e^q$ .

Replacing Young's modulus  $E$  with  $\rho_e^q E$  results in that the stiffness tensor and the global stiffness matrix needs to be replaced. The new stiffness matrix takes the form

$$\mathbf{K}(\boldsymbol{\rho}) = \sum_{e=1}^n \rho_e^q \mathbf{K}_e^0. \quad (2.21)$$

The convex approximation  $g^{SIMP}$  used in the SIMP method is derived in the same way as  $g^{OC}$  is derived in the OC method. This means that equations (2.9) and (2.10) are still valid but due to the changed stiffness matrix does the derivative of  $g_0$  change from equation (2.17) to

$$\frac{\partial g_0(\boldsymbol{\rho})}{\partial \rho_e} = -\mathbf{u}_e^T q \rho_e^{q-1} \mathbf{K}_e^0 \mathbf{u}_e \quad (2.22)$$

This implies that the convex approximation  $g_0^{SIMP}$  is defined by:

$$g_0^{SIMP}(\boldsymbol{\rho}) = \xi + \sum_{e=1}^n b_e^k \rho_e^{-\alpha} \quad (2.23)$$

$$\text{where } b_e^k = \frac{1}{\alpha} ((\mathbf{u}_e^k)^T q (\rho_e^k)^{q-1} \mathbf{K}_e^0 \mathbf{u}_e^k) (\rho_e^k)^{1+\alpha}. \quad (2.24)$$

where  $\xi = g_0^{SIMP}(0)$  once again is constant and of no interest during our optimization.

### 2.1.3 Calculating the optimal construction

Finding the optimal structure the SIMP method makes use of the KKT method which is a well known mathematical optimization method.

## Karush-Kuhn-Tucker (KKT)

An important cornerstone when defining the KKT method is the Lagrangian,  $\mathcal{L}$ , which is defined by

$$\mathcal{L}(x, \lambda) = g_0(x) + \sum_{i=1}^l \lambda_i g_i(x) \quad (2.25)$$

where  $\lambda_i$  denotes the Lagrangian multipliers. The KKT method states that a stationarity point to the Lagrangian is found when the following conditions are fulfilled

$$\frac{\partial \mathcal{L}(x, \lambda)}{\partial x_j} = \frac{\partial g_0(x)}{\partial x_j} + \sum_{i=1}^l \lambda_i \frac{\partial g_i(x)}{\partial x_j} = 0 \quad (2.26)$$

$$\lambda_i g_i(x) = 0 \quad (2.27)$$

$$g_i(x) \leq 0 \quad (2.28)$$

$$\lambda_i \geq 0 \quad (2.29)$$

for all  $j = 1, \dots, n$  and  $i = 1, \dots, l$  where  $l$  is the number of constraint functions and  $n$  is the number of variables  $x_j$ . Combining equations (2.25) and (2.27) it is clear that if this stationary point minimizes  $\mathcal{L}$  it will also minimize the objective function  $g_0$ .

An important lemma, that is used to derive the SIMP method, and that follows from these conditions is defined as

**Lemma 1** *Let  $\mathbb{P}$  be a convex problem, and let  $(x^*, \lambda^*)$  be a KKT point of  $\mathbb{P}$ . Then  $x^*$  is a global minimum of  $\mathbb{P}$ .*

From the KKT method another optimization method has been developed which uses the Lagrangian Duality to obtain an optimal solution. This method states that

$$\min_{x \in \mathbb{R}^m} \max_{0 \leq \lambda} \mathcal{L}(x, \lambda) = \min_{x \in \mathbb{R}^m} \max_{0 \leq \lambda} \left\{ g_0(x) + \sum_{i=1}^l \lambda_i g_i(x) \right\} \quad (2.30)$$

and gives an optimal solution that fulfill the KKT conditions on a convex problem. The dual problem  $\mathbb{D}$  corresponding to the primal problem  $\mathbb{P}$  is obtained by.

$$\mathbb{D} = \begin{cases} \max_{\lambda} \varphi(\lambda) \\ s.t. \ 0 \leq \lambda \end{cases} \quad (2.31)$$

where the dual objective function  $\varphi$  is defined as

$$\varphi(\lambda) = \min_{\mathbf{x} \in \mathbb{R}^m} \mathcal{L}(\mathbf{x}, \lambda). \quad (2.32)$$

For more information about the KKT method see [7].

For the current problem stated in (2.5) the Lagrangian,  $\mathcal{L}$ , becomes

$$\mathcal{L}(\boldsymbol{\rho}, \lambda) = g_0^{SIMP}(\boldsymbol{\rho}) + \lambda g_1^{SIMP}(\boldsymbol{\rho}) = \sum_{e=1}^n b_e^k \rho_e^{-\alpha} + \lambda \left( \sum_{e=1}^n a_e \rho_e t_h - \lambda V \right). \quad (2.33)$$

From this the dual objective function is defined as the minimum of the Lagrangian i.e.

$$\varphi(\lambda) = \min_{\rho_{min} \leq \rho_e \leq \rho_{max}} \mathcal{L}(\boldsymbol{\rho}, \lambda) = \sum_{e=1}^n \min[b_e^k \rho_e^{-\alpha} + \lambda a_e \rho_e t_h] - \lambda V. \quad (2.34)$$

$$\text{where } b_e^k = \frac{1}{\alpha} (\mathbf{u}_e^k)^T q \rho_e^{q-1} \mathbf{K}_e^0 \mathbf{u}_e^k (\rho_e^k)^{1+\alpha} \quad (2.35)$$

cf.[1]

Clearly the minimum of the  $\mathcal{L}$  occurs simultaneously with  $\mathcal{L}_\alpha = b_e^k \rho_e^{-\alpha} + \lambda a_e \rho_e$  having its minimum. This minimum occurs either when  $\rho_e = \rho^{min}$ , when  $\rho_e = \rho^{max}$  or in the interval  $\rho^{min} \leq \rho_e \leq \rho^{max}$ . Assuming that this occurs within the interval  $\rho^{min} \leq \rho_e \leq \rho^{max}$  is  $\rho_e$  found through

$$\frac{\partial \mathcal{L}_\alpha}{\partial \rho_e} = -\alpha b_e^k \rho_e^{-\alpha-1} + \lambda a_e t_h \Rightarrow \rho_e = \left( \frac{\alpha b_e^k}{\lambda a_e t_h} \right)^\eta \quad (2.36)$$

where  $\eta = \frac{1}{1+\alpha}$ . Through this an iteration scheme for finding the optimum structure is constructed as

$$\rho_e^{k+1} = \min \left\{ \max \left[ \rho_e^k \left( \frac{(\mathbf{u}_e^k)^T q \rho_e^{q-1} \mathbf{K}_e^0 \mathbf{u}_e^k}{\lambda a_e t_h} \right)^\eta, \rho_{min} \right], \rho_{max} \right\} \quad (2.37)$$

$$\frac{\partial \varphi}{\partial \lambda} = \sum_{e=1}^n a_e \rho_e t_h - V = 0 \quad (2.38)$$

This scheme is then repeated until the optimized state is reached.

For a more theory about the SIMP method see[1].

### 2.1.4 Results from using the SIMP method

In this section the outcome of a SIMP simulation is shown. During the simulations the following parameter values were used

penalization constant $q$	intervening variable constant $\alpha$	initial density $\rho_e^0$
3	3	$0.3 \forall e$

and if nothing else is mentioned a grid of 60x40 4-node isoparametric elements were used i.e. 2400 elements.

To start the analysis the changes in the distribution of material over the iterations will be discussed. In Figure 2.4(a) the solution after 5 iterations and 200 iterations are shown.

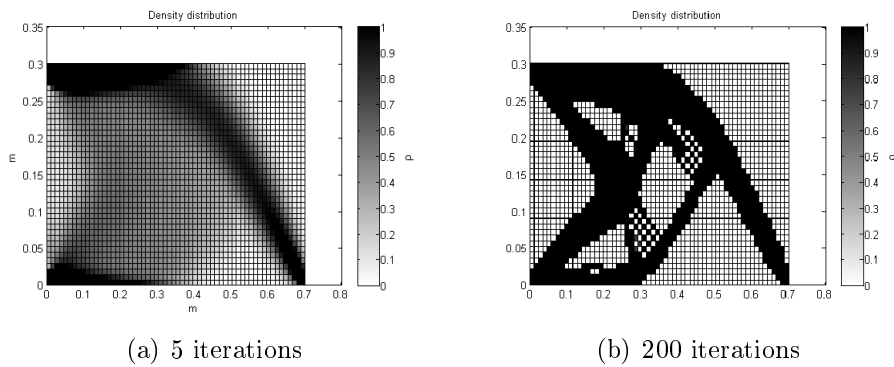


Figure 2.4: Distribution of material after 5 iterations and after 200 iterations

In Figure 2.4 one clearly see how the penalization force the densities to  $\rho_e \in \{0, 1\}$ .

The evolution of the compliance over the number of iterations is illustrated in Figure 2.5

Figure 2.5 is zoomed in on the first 20 iterations since it turned out to be here the main changes occurred in the compliance. From this figure it is clear that the structure becomes stiffer as the optimization proceeds.

Finally the influence of using different meshes is considered. In Figure 2.6a. simulations has been performed on a space discretization of 25X24 four node elements i.e. 600 elements and in Figure 2.6b. on 60X40 four node elements.

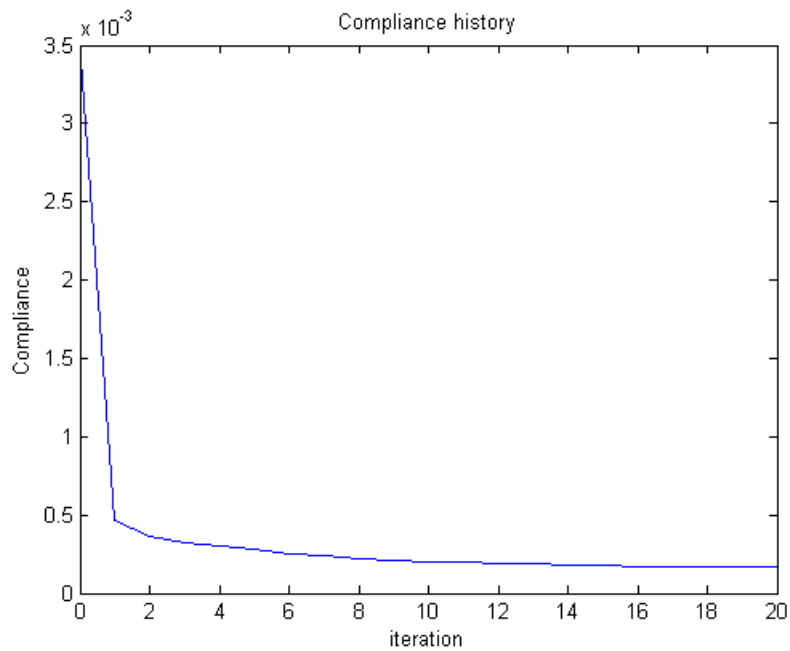
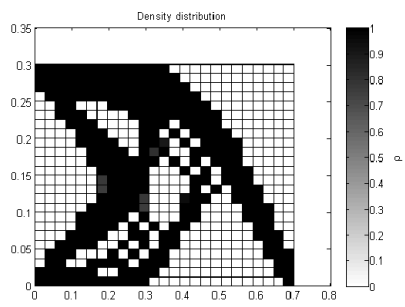
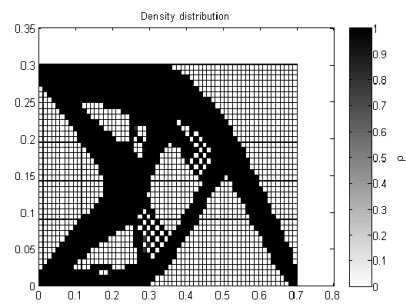


Figure 2.5: Evolution of the compliance over the number of iterations

After using different meshes during the simulations it can be concluded that the solutions converged towards the same "main" shape but still differ significantly. This is an effect of mesh dependency present in the SIMP method. Referring to Figure 2.6 one can conclude that a finer mesh results in a structure with very thin threads. This property will be enhanced when finer meshes are used. This is an example of that the SIMP method has no unique solution. In the next part, Part B, a new method is derived for which this mesh dependency is circumvented.



(a) Coarse mesh



(b) Fine mesh

Figure 2.6: Influence of using different space discretization

# Chapter 3

## Part B

### 3.1 Topology optimization based on Cahn-Hilliard equation

The SIMP method is, as recently mentioned, associated with a defect in the sense that it generates a solution that is mesh dependent. In this section a method that introduce a length scale into the problem is derived. This introduced length scale will have the effect of eliminating the mesh dependency.

The derivation of this new method starts with the defining of the objective functional and the constraints so that the optimization problem  $\mathcal{P}^B$  can be formed.

#### 3.1.1 Defining the optimization problem $\mathcal{P}^B$

The objective functional of this method is denoted  $E$  and derived with a base consisting of the strain energy denoted  $w$ . The expression of the strain energy was stated in equation (1.26) and is stated once more

$$w = \frac{1}{2} \varepsilon_{ij} D_{ijkl} \varepsilon_{kl}. \quad (3.1)$$

To avoid non physical concentrations such as,  $\rho \notin [0, 1]$ , and also add a penalization of intermediate concentrations a penalization function  $F(\rho)$  is added to  $E$ , where  $F(\rho)$  is illustrated in Figure 3.1 and defined as

$$F(\rho) = (\rho^2(1 - \rho)^2 e^{15(0.5 - \rho)^2} + \rho^2(1 - \rho)^2)10 \quad (3.2)$$

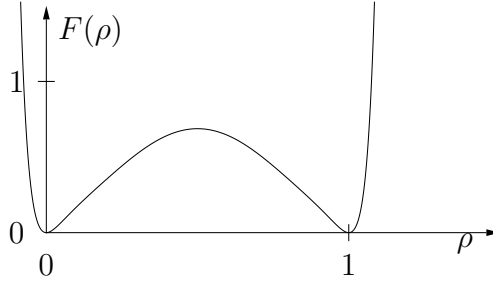


Figure 3.1: Illustration of  $F(\rho)$ .

A consequence of introducing the penalization function  $F(\rho)$  is that the method becomes mesh dependent. To resolve this issue another penalization function with the aim of penalizing all gradients  $\rho_{,i}$  is introduced. This second penalization function is denoted  $S$  and defined by

$$S(\rho) = \int_{\Omega} \rho_{,i} \rho_{,i} d\Omega \quad (3.3)$$

Collecting equations (3.1), (3.2) and (3.3) the objective functional  $E(\rho, \rho_{,i}, \mathbf{u})$  is defined

$$E(\rho, \rho_{,i}, \mathbf{u}) = \int_{\Omega} (F(\rho) + \frac{\gamma}{2} \rho_{,i} \rho_{,i}) d\Omega + \eta \int_{\Omega} w(\rho, \epsilon_{ij}) d\Omega \quad (3.4)$$

where  $\eta$  is a weight inserted to even the relation between the different parts of the functional. The parameter,  $\gamma$ , is introduced to define a length scale into the problem. The effect of changing  $\gamma$  can be described as:

- Smaller  $\gamma \Rightarrow$  slim interface between material and no material
- Bigger  $\gamma \Rightarrow$  wider interface between material and no material

Since  $F(\rho) \geq 0$ ,  $\rho_{,i} \rho_{,i} \geq 0$  and  $w(\rho, \epsilon_{ij}) \geq 0$  it can be concluded that  $E(\rho, \rho_{,i}, \mathbf{u})$  is bounded by the lower limit  $E(\rho, \rho_{,i}, \mathbf{u}) > \xi$  where  $\xi > 0$ . Note that the objective functional  $E$  is not a convex functional, this is easily seen by looking at the first term  $F(\rho)$  illustrated in Figure 3.1. This means that it can not be guaranteed that a stationary point occurs in the global minimum but merely that it is placed in a local minimum.

Connecting to phase-field models an interpretation of  $E(\rho, \rho_{,i}, \mathbf{u})$  is that it represents the total energy of the structure and that the main goal is to lower this energy as much as possible. With this interpretation  $F(\rho)$  defines the bulk energy or the cost of intermediate material densities and  $\frac{\gamma}{2} \rho_{,i} \rho_{,i}$  defines the surface energy or the cost of creating surfaces.

In the next section equilibrium and volume constraints is discussed since these must be enforced when minimizing  $E(\rho, \rho_{,i}, \mathbf{u})$

## Constraints

The amount of material available for the design is given by  $V_0$  which implies a volume constraint  $g_1$  given by

$$g_1 = \int_{\Omega} \rho_e t_h d\Omega - V_0 \leq 0 \quad (3.5)$$

recall that  $t_h$  denotes the maximum thickness of the structure.

To fulfill the local form of the static equilibrium equations the constraints  $g_\alpha$  are imposed

$$g_\alpha = \sigma_{kl,l} + b_k = 0 \quad \alpha = 2, 3, 4 \quad (3.6)$$

With the objective function (3.4) and the constraints (3.5), (3.6) the new optimization problem denoted  $\mathcal{P}^B$  is formulated as

$$\mathcal{P}^2 = \begin{cases} \min_{\rho} E(\rho, \rho, \mathbf{u}) \\ \text{s.t. } g_i \leq 0 \end{cases} \quad (3.7)$$

The idea is now to define a Lagrangian,  $\mathcal{L}$ , and then seek a stationarity point. The Lagrangian,  $\mathcal{L}$ , for the current problem is defined by inserting the objective function (3.4) and the constraints (3.5), (3.6) into the definition of the Lagrangian (2.25) which results in

$$\mathcal{L}(\rho, \rho, \mathbf{u}, \boldsymbol{\lambda}^k, \lambda^c) = E(\rho, \rho, \mathbf{u}) + \int_{\Omega} \lambda_k^i g_i d\Omega + \lambda^c g_1. \quad (3.8)$$

where  $\lambda_k^i$  and  $\lambda^c$  denotes the Lagrangian multipliers. Note that  $\lambda^c$  is constant over the hole domain  $\Omega$ , this is a property that will be useful further down in this thesis.

In the next section is the present stiffness tensor defined.

## Stiffness tensor

As previously mentioned in Section 1.2 is the stiffness tensor defined by

$$D_{ijkl} = \tilde{f} D_{ijkl}^0 \quad (3.9)$$

where  $\tilde{f}$  is a function depending on  $\rho$  and  $D_{ijkl}^0$  is an isotropic fourth order tensor defined by

$$D_{ijkl}^0 = 2G \left[ \frac{1}{2} (\delta_{ik} \delta_{jl} + \delta_{il} \delta_{jk}) + \frac{\nu}{1 - 2\nu} \delta_{ij} \delta_{kl} \right] \quad (3.10)$$

For the SIMP method was  $\tilde{f}$  defined as  $\tilde{f}(\rho) = \rho^q$  which led to a penalization of intermediate concentrations. Since the intermediate concentrations already are penalized by  $F(\rho)$  is a linear relation between concentration and element stiffness sought. Setting  $\tilde{f}(\rho) = \rho$  would however lead to singularities and to avoid these  $\tilde{f}$  is instead defined as

$$\tilde{f} = \frac{\rho}{1 + e^{-40\rho}} + \xi \quad (3.11)$$

where  $\xi$  should be seen as the residual stiffness and has during implementation been set to  $\xi = 0.01$  An illustration of  $\tilde{f}$  is shown in Figure 3.2

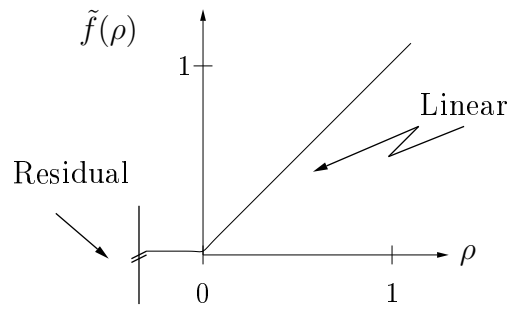


Figure 3.2: Illustration of the residual stiffness function  $\tilde{f}$

From this figure it is clear that

$$\tilde{f}(\rho) > 0 \quad \forall \rho \quad (3.12)$$

which is a property of  $\tilde{f}$  that will lead to that singularities are avoided, this will be discussed more later.

### 3.1.2 Deriving the stationarity point

The Lagrangian,  $\mathcal{L}$ , associated with the problem was previously defined as

$$\mathcal{L}(\rho, \rho_{,i}, \mathbf{u}, \boldsymbol{\lambda}^k, \lambda^c) = E(\rho, \rho_{,i}, \mathbf{u}) + \int_{\Omega} \lambda_i^k g_i d\Omega + \lambda^c g_1. \quad (3.13)$$

wich after inserting definitions (3.4), (3.5) and (3.6) reads

$$\begin{aligned} \mathcal{L}(\rho, \rho_{,i}, \mathbf{u}, \boldsymbol{\lambda}^k, \lambda^c) = & \int_{\Omega} (F(\rho) + \frac{\gamma}{2}(\rho_{,i})^2) d\Omega + \eta \int_{\Omega} w(\rho, \epsilon_{ij}) d\Omega + \\ & \int_{\Omega} \lambda_i^k (\sigma_{il,l} + b_i) d\Omega + \int_{\Omega} \lambda^c \rho t_h d\Omega - \lambda^c V_0. \end{aligned} \quad (3.14)$$

Using Green-Gauss's theorem on the third integral and using the boundary condition  $\rho_{,j} n_j = 0$  along  $\partial\Omega$  results in

$$\begin{aligned} \mathcal{L}(\rho, \rho_{,i}, \mathbf{u}, \boldsymbol{\lambda}^k, \lambda^c) = & \int_{\Omega} (F(\rho) + \frac{\gamma}{2}(\rho_{,i})^2) d\Omega + \eta \int_{\Omega} w(\rho, \epsilon_{ij}) d\Omega + \\ & \int_{\Omega} \lambda_i^k b_i d\Omega + \int_{\partial\Omega} t_i \delta \lambda_i^k d\partial\Omega - \int_{\Omega} \sigma_{ij} \delta \lambda_{i,j}^k d\Omega + \int_{\Omega} \lambda^c \rho t_h d\Omega - \lambda^c V_0. \end{aligned} \quad (3.15)$$

To be able to find a stationary point of the functional  $\mathcal{L}$  use is made of calculus of variation which states that the stationarity point is defined by its variations being equal to zero i.e.

$$\frac{\delta \mathcal{L}}{\delta \rho} \delta \rho + \frac{\delta \mathcal{L}}{\delta \rho_{,i}} \delta \rho_{,i} = 0 \quad \frac{\delta \mathcal{L}}{\delta u_e} \delta u_e = 0 \quad \frac{\delta \mathcal{L}}{\delta \lambda_e^k} \delta \lambda_e^k = 0 \quad \frac{\delta \mathcal{L}}{\delta \lambda^c} \delta \lambda^c = 0 \quad (3.16)$$

Applying this to the Lagrangian functional (3.15) results in

$$\begin{aligned} & \frac{\delta \mathcal{L}}{\delta \rho} \delta \rho + \frac{\delta \mathcal{L}}{\delta \rho_{,i}} \delta \rho_{,i} = 0 \\ = & \int_{\Omega} (F'_{,\rho} \delta \rho + \gamma \rho_{,i} \delta \rho_{,i} - \tilde{f}'_{\rho} D_{ijkl}^0 \epsilon_{kl} \lambda_{i,j}^k \delta \rho + \lambda^c t_h \delta \rho + \eta w'_{,\rho} \delta \rho) d\Omega \end{aligned} \quad (3.17)$$

$$\frac{\delta \mathcal{L}}{\delta u_e} \delta u_e = \eta \int_{\Omega} w'_{,\epsilon_{kl}} \delta \epsilon_{kl} d\Omega - \int_{\Omega} D_{ijkl} \delta \epsilon_{kl} \lambda_{i,j}^k d\Omega = 0. \quad (3.18)$$

$$\frac{\delta \mathcal{L}}{\delta \lambda_e^k} \delta \lambda_e^k = \int_{\Omega} \delta \lambda_e^k b_e d\Omega + \int_{\partial\Omega} t_e \delta \lambda_e^k d\partial\Omega - \int_{\Omega} \sigma_{el} \delta \lambda_{e,l}^k d\Omega = 0 \quad (3.19)$$

$$\frac{\delta \mathcal{L}}{\delta \lambda^c} \delta \lambda^c = \left( \int_{\Omega} \rho t_h d\Omega - V_0 \right) \delta \lambda^c = 0 \quad (3.20)$$

For the interested reader we recommend reading [5] or [4].

Rearranging (3.18) results in

$$\int_{\Omega} (\eta w'_{,\varepsilon_{kl}} - D_{ijkl} \lambda_{i,j}^k) \delta \varepsilon_{kl} d\Omega = 0 \quad (3.21)$$

From this relation it is concluded that the choice

$$\eta w'_{,\varepsilon_{kl}} = D_{ijkl} \lambda_{i,j}^k \Rightarrow \lambda_{i,j}^k = \eta C_{ijkl} w'_{,\varepsilon_{kl}} \quad (3.22)$$

results in that

$$\frac{\partial \mathcal{L}}{\partial u_e} \delta u_e = 0 \quad (3.23)$$

Note that the compliance tensor  $C_{ijkl} = D_{ijkl}^{-1}$  was introduced. Inserting expression (3.22) for the Lagrange multiplier  $\lambda_{i,j}^k$  into (3.17) results in

$$\int_{\Omega} (F'_{,\rho} \delta \rho + \gamma \rho_{,i} \delta \rho_{,i} - \tilde{f}'_{\rho} D_{ijkl}^0 \varepsilon_{kl} C_{ijpn} \eta w'_{,\varepsilon_{pn}} \delta \rho + \lambda^c t_h \delta \rho + \eta w'_{,\rho} \delta \rho) d\Omega = 0 \quad (3.24)$$

Two of the terms from Equation (3.24) are now rewritten as

$$\tilde{f}'_{\rho} D_{ijkl}^0 \varepsilon_{kl} C_{ijpn} \eta w'_{,\varepsilon_{pn}} = \eta \frac{\tilde{f}'_{\rho}}{\tilde{f}} \varepsilon_{ij} w'_{,\varepsilon_{ij}} \quad (3.25)$$

$$\rho_{,i} \delta \rho_{,i} = (\rho_{,i} \delta \rho)_{,i} - \rho_{,ii} \delta \rho \quad (3.26)$$

Applying Green-Gauss's theorem together with these reformulated terms gives

$$\int_{\Omega} (F'_{,\rho} \delta \rho - \gamma \rho_{,ii} \delta \rho - \eta \frac{\tilde{f}'_{\rho}}{\tilde{f}} \varepsilon_{ij} w'_{,\varepsilon_{ij}} \delta \rho + \lambda^c t_h \delta \rho + \eta w'_{,\rho} \delta \rho) d\Omega = 0 \quad (3.27)$$

$$w'_{,\rho} = \frac{\tilde{f}'_{\rho}}{\tilde{f}} w \quad (3.28)$$

$$w'_{,\varepsilon_{ij}} \varepsilon_{ij} = 2w \quad (3.29)$$

This means that the objective function, see Equation (3.4), will have a local optimum when

$$\mu = -\lambda^c t_h = \frac{\partial F}{\partial \rho} - \gamma \rho_{,ii} - \eta \tilde{g}(\rho, \mathbf{u}_e) \quad (3.30)$$

where  $\tilde{g}$  is defined by

$$\tilde{g} = \frac{\tilde{f}'_{\rho}}{\tilde{f}} w \quad (3.31)$$

Note that  $\lambda^c$  is a constant which means that our local minimum occurs at a state where  $\mu$  is constant over the whole domain  $\Omega$ . During the simulations this is used to see if the solution has converged. Also note that comparing equations (2.29) and (3.30) it is seen that  $\mu < 0$  when an optimum is found. In equation (3.31) the possible singularities discussed in Section 3.1.1 are observed.

An extrema that fulfill (3.30) shall now be sought using the Cahn-Hilliard equation which describes the diffusion of material over time.

### 3.1.3 Cahn-Hilliards Equation Three node elements

The Cahn-Hilliard equation is defined by:

$$\dot{\rho} + J_{j,j} = 0 \quad (3.32)$$

along with the boundary conditions

$$\rho_{,j}n_j = \mu_{,j}n_j = 0 \quad \text{along } \partial\Omega \quad (3.33)$$

where the flux vector  $J_j$  is defined as

$$J_j = -M(\rho)\mu_{,j} \quad (3.34)$$

and  $M$  denotes the mobility.

A property that follows from using the Cahn-Hilliard equation appears after inserting equation (3.32) into (3.5) which results in

$$\dot{V} = \int_{\Omega} \dot{\rho}t_h dV = - \int_{\partial\Omega} J_i n_i t_h dS = 0 \quad (3.35)$$

where use have been made of equation (3.32), *Gauss theorem* as well as the boundary condition (3.33). Equation (3.35) tells us is that using Cahn-Hilliards equation results in that the method conserves the amount of material.

To motivate why use is being made of Cahn-Hilliard equation the rate of the functional  $\Psi = \frac{\partial \mathcal{L}}{\partial t}$  is derived, i.e.

$$\begin{aligned} \Psi = & \int_{\Omega} \left( \frac{\partial F}{\partial \rho} - \gamma_{\rho,ii} - \lambda_{i,j}^e \tilde{f}'_{\rho} D_{ijkl}^0 \varepsilon_{kl} + \eta \tilde{g} \right) \frac{d\rho}{dt} d\Omega + \lambda^c \int_{\Omega} \frac{d\rho}{dt} t_h d\Omega + \\ & \int_{\Omega} \left( \eta \frac{\partial w}{\partial \varepsilon_{kl}} - \lambda_{i,j}^k D_{ijkl} \right) \frac{d\varepsilon_{kl}}{dt} d\Omega + \int_{\Omega} (\sigma_{i,j,j} + b_i) \frac{d\lambda_i^k}{dt} d\Omega + \left( \int_{\Omega} \rho t_h d\Omega - V_0 \right) \frac{d\lambda^c}{dt} \end{aligned} \quad (3.36)$$

Rewriting equation (3.36), together with (3.35), (3.22) and imposing the present constraints (3.5), (3.6) gives

$$\Psi = \int_{\Omega} \left( \frac{\partial F}{\partial \rho} - \gamma_{\rho,ii} - \eta \frac{\tilde{f}'_{\rho}}{f} \sigma_{ij} C_{ijkl} 2w + \eta \tilde{g} \right) \frac{d\rho}{dt} d\Omega \quad (3.37)$$

where use have been made of the relation

$$\varepsilon_{kl} \frac{\partial w}{\partial \varepsilon_{kl}} = 2w \quad (3.38)$$

Equation (3.31) states that  $\tilde{g} = \frac{f'_e}{f}w$  which rewrites equation (3.37) into

$$\Psi = \int_{\Omega} \left( \frac{\partial F}{\partial \rho} - \gamma \rho_{,ii} - \eta \tilde{g} \right) \frac{d\rho}{dt} d\Omega = \int_{\Omega} \mu \frac{d\rho}{dt} d\Omega \quad (3.39)$$

which after making use of the product rule and *Gauss theorem* results in

$$\Psi = \int_{\Omega} \mu (M \mu_{,i})_{,i} dt d\Omega = - \int_{\Omega} \mu_{,i} M \mu_{,i} dt d\Omega + \int_{\partial\Omega} \mu M \mu_{,i} n_i dt d\partial\Omega \quad (3.40)$$

Finally using the boundary condition  $\mu_{,i} n_e = 0$  on  $\partial\Omega$  defines the rate of the functional  $\Psi$  as

$$\Psi = - \int_{\Omega} \mu_{,i} M \mu_{,i} d\Omega \leq 0 \quad (3.41)$$

From equation (3.41) it is concluded that if the mobility is chosen as  $M(\rho) > 0$  the method will guide the solution to a state that minimizes the Lagrangian and therefore also minimizing the functional  $E$ , cf. (3.4).

Making use of Cahn-Hilliard equations imposes that a discretization in time is needed for a numerical implementation. The discretization in time is in this thesis chosen as

$$\dot{\rho} \approx \frac{\rho - \rho_n}{\Delta t} \quad (3.42)$$

where the  $\rho_n$  represents the old state value and  $\Delta t$  the time increment between the old state and the current state

### 3.1.4 Finite element formulation

In Section 3.1.2 equation (3.30) was derived which needed to be fulfilled in order for  $E(\rho, \rho_{,i}, \mathbf{u})$  to have a stationarity point. To reach this stationarity point and also making sure that it is a local minimum Cahn-Hilliards equation (3.32) is used. These two equations are now together the local equilibrium equations (3.6) going to define three strong forms from which the residuals  $\mathbf{f}_1$ ,  $\mathbf{f}_2$  and  $\mathbf{f}_3$  are derived. The residual originated from the local equilibrium equations has already been derived in Section 1.2 and is now denoted  $\mathbf{f}_3$  i.e.

$$\mathbf{f}_3 = \int_{\Omega} \mathbf{B}_m^T \mathbf{D} \mathbf{B}_m d\Omega \mathbf{u} - \mathbf{P} \quad (3.43)$$

cf. (1.11)- (1.13)

#### Strong forms

The other two strong forms defined by equations (3.30) and (3.32) are stated as

$$\dot{\rho} + J_{j,j} = 0 \quad (3.44)$$

$$\frac{\partial F}{\partial \rho} - \gamma \rho_{,ii} - \eta \tilde{g}(\rho, u_e) - \mu = 0. \quad (3.45)$$

#### Weak forms

Multiplying equations (3.44) and (3.45) with the weight functions  $\bar{\varphi}_l$  and  $\bar{\mu}_l$  and integration over the domain  $\Omega$  the following is obtained

$$\int_{\Omega} \bar{\varphi}_l \dot{\rho} d\Omega + \int_{\Omega} \bar{\varphi}_l J_{j,j} d\Omega = 0 \quad (3.46)$$

$$\int_{\Omega} \bar{\mu}_l \frac{\partial F}{\partial \rho} d\Omega - \int_{\Omega} \bar{\mu}_l \gamma \rho_{,ii} d\Omega - \int_{\Omega} \bar{\mu}_l \eta \tilde{g} d\Omega - \int_{\Omega} \bar{\mu}_l \mu d\Omega = 0 \quad (3.47)$$

Which after making use of the boundary condition  $\rho_{,j} n_j = 0$ , the product rule

$$\text{Chain rule } (\bar{\varphi}_l J_j)_{,j} = \bar{\varphi}_{l,j} J_j + \bar{\varphi}_l J_{j,j} \quad (3.48)$$

and *Gauss theorem* (1.6) results in

$$\int_{\Omega} \bar{\varphi}_l \dot{\rho} d\Omega - \int_{\Omega} \bar{\varphi}_{l,j} J_j d\Omega + \int_{\partial\Omega} \bar{\varphi}_l J_j n_j d\partial\Omega = 0 \quad (3.49)$$

$$\int_{\Omega} \bar{\mu}_l \frac{\partial F}{\partial \rho} d\Omega + \int_{\Omega} \bar{\mu}_{l,i} \gamma \rho_{,i} d\Omega - \int_{\Omega} \bar{\mu}_l \eta \tilde{g} d\Omega - \int_{\Omega} \bar{\mu}_l \mu d\Omega = 0. \quad (3.50)$$

Insertion of the boundary condition  $J_j n_j = 0$  and the time discretization defined in equation (3.42) rewrites equation (3.49) into

$$\int_{\Omega} \bar{\varphi}_l (\rho - \rho_n) d\Omega - \Delta t \int_{\Omega} \bar{\varphi}_{l,j} J_j d\Omega = 0. \quad (3.51)$$

which together with equation (3.50) defines the two weak forms of the residuals  $\mathbf{f}_1$  and  $\mathbf{f}_2$ .

### Finite element formulation

Deriving the finite element formulations that originates from these weak forms the field variables are approximated as

$$\rho = \mathbf{N} \boldsymbol{\rho} \quad \nabla \rho = \mathbf{B} \boldsymbol{\rho}_e \quad (3.52)$$

$$\mu = \mathbf{N} \boldsymbol{\mu} \quad \nabla \mu = \mathbf{B} \boldsymbol{\mu}_e \quad (3.53)$$

$$\mathbf{u} = \mathbf{N}_m \mathbf{u}_e \quad \boldsymbol{\varepsilon} = \mathbf{B}_m \mathbf{u}_e \quad (3.54)$$

where using Galerkins method when choosing the weight functions results in

$$\bar{\varphi}_l = \mathbf{N} \bar{\boldsymbol{\varphi}} \quad \nabla \bar{\varphi} = \mathbf{B} \bar{\boldsymbol{\varphi}} \quad (3.55)$$

$$\bar{\mu}_l = \mathbf{N} \bar{\boldsymbol{\mu}} \quad \nabla \bar{\mu} = \mathbf{B} \bar{\boldsymbol{\mu}} \quad (3.56)$$

Inserting these approximations into equations (3.50) and (3.51) defines the residuals as

$$\mathbf{f}_1 = \int_{\Omega} \mathbf{N}^T (\boldsymbol{\rho} - \boldsymbol{\rho}_n) d\Omega + \Delta t \int_{\Omega} \mathbf{B}^T M \nabla \boldsymbol{\mu} d\Omega \quad (3.57)$$

$$\mathbf{f}_2 = \int_{\Omega} \mathbf{N}^T \frac{\partial F}{\partial \rho} \frac{1}{\epsilon} d\Omega + \epsilon \int_{\Omega} \mathbf{B}^T \nabla \boldsymbol{\rho} d\Omega - \eta \int_{\Omega} \mathbf{N}^T \tilde{g} d\Omega - \int_{\Omega} \mathbf{N}^T \boldsymbol{\mu} d\Omega. \quad (3.58)$$

where use have been made of the definition of the flux vector  $J_j = -M(\rho) \mu_{,j}$

The shape functions used in the approximations of the field variables are defined by the theory based on triangular coordinates.

### 3.1.5 Three-Node Triangles

This section will describe the interpolation of a three-node triangle element. There are many ways to do this but here the interpolation is based on the triangular coordinates  $L_1$ ,  $L_2$  and  $L_3$ . The coordinate  $L_i$  is best described as a straight line opposite the  $i^{th}$  corner in the triangle, see Figure 3.3a,b.

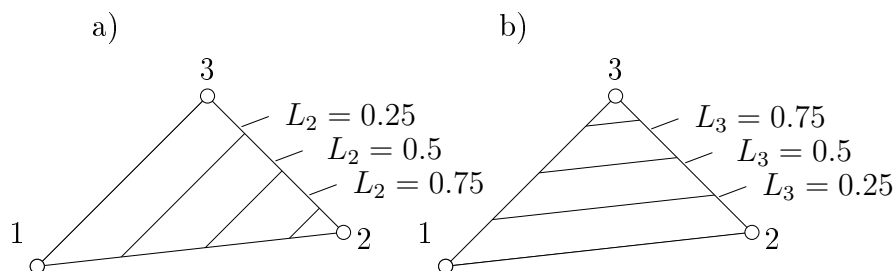


Figure 3.3: Illustration of natural coordinates a)  $L_2$  b)  $L_3$ .

The triangular coordinates  $L_1$ ,  $L_2$  and  $L_3$  are related to the Cartesian system through

$$x = L_1x_1 + L_2x_2 + L_3x_3 \quad (3.59)$$

$$y = L_1y_1 + L_2y_2 + L_3y_3 \quad (3.60)$$

$$1 = L_1 + L_2 + L_3 \quad (3.61)$$

Solving this system of equations for  $x$  and  $y$  gives the triangular coordinates  $L_1$ ,  $L_2$  and  $L_3$  expressed in the Cartesian coordinates  $x$  and  $y$  as

$$L_i = \frac{a_i + b_i x + c_i y}{2A_e} \quad (3.62)$$

Where  $A_e$  denotes the element area and the variables  $a_i$ ,  $b_i$  and  $c_i$  are described by

$$a_1 = x_2y_3 - x_3y_2 \quad (3.63)$$

$$b_1 = y_2 - y_3 \quad (3.64)$$

$$c_1 = x_3 - x_2 \quad (3.65)$$

etc. with cyclic rotation of indices 1,2 and 3. When using triangular elements

with only three nodes the shape functions are conveniently defined as

$$N_i = L_i \quad i = 1 \dots 3 \quad (3.66)$$

$$\mathbf{N} = [N_1 \ N_2 \ N_3] \quad (3.67)$$

$$\mathbf{N}_m = \begin{pmatrix} N_1 & 0 & N_2 & 0 & N_3 & 0 \\ 0 & N_1 & 0 & N_2 & 0 & N_3 \end{pmatrix} \quad (3.68)$$

Referring to (3.62)  $\mathbf{B} = \nabla \mathbf{N}$  and  $\mathbf{B}_m = \tilde{\nabla}^T \mathbf{N}_m$  are defined by

$$\mathbf{B} = \nabla \mathbf{N} = \frac{1}{2A_e} \begin{pmatrix} b_1 & b_2 & b_3 \\ c_1 & c_2 & c_3 \end{pmatrix} \quad (3.69)$$

$$\mathbf{B}_m = \tilde{\nabla}^T \mathbf{N}_m = \frac{1}{2A_e} \begin{pmatrix} b_1 & 0 & b_2 & 0 & b_3 & 0 \\ 0 & c_1 & 0 & c_2 & 0 & c_3 \\ b_1 & c_1 & b_2 & c_2 & b_3 & c_3 \end{pmatrix} \quad (3.70)$$

where  $\tilde{\nabla}$  is defined in Section 3.2.

Note that this means that  $\mathbf{B}$  and  $\mathbf{B}_m$  are constant which will turn out to be a useful property. For discussion related to the triangular coordinates see [2]

Numerical integration is needed to be able to solve the integrations present in the finite element formulation.

## Numerical Integration

The numerical integration of a function  $f$  over a triangle with the area  $A_e$  is formed in the following way

$$\int \int_{A_e} f dA_e = A_e \sum_{i=1}^n w_i f(L_1, L_2, L_3) \quad (3.71)$$

where  $n$  is the number of integration points, in our case we have through test runs come to the conclusion that  $n = 9$  integration points are sufficient. The 9 integration points are together with their weights  $w_i$  found in Table 1 cf. [3]. Figure 3.4 illustrates the placement of the integration points.

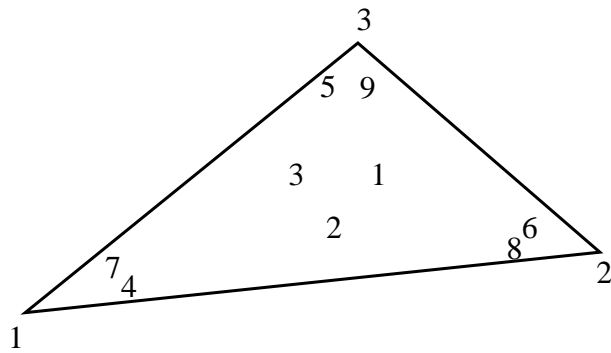


Figure 3.4: Placement of the nine Gauss points

## Linearization

The construction of the global stiffness matrix used in the numerical implementation of the method will now be derived from the linearization of the residuals derived in Section 3.1.4. Linearization of  $\mathbf{f}_1$ ,  $\mathbf{f}_2$  and  $\mathbf{f}_3$  results in

$$d\mathbf{f}_1 = \int_{\Omega} (\mathbf{N}^T + \Delta t \mathbf{B}^T \nabla \boldsymbol{\mu}_e \frac{\partial M}{\partial \rho}) d\boldsymbol{\rho} d\Omega + \Delta t \int_{\Omega} \mathbf{B}^T M \nabla d\boldsymbol{\mu} d\Omega \quad (3.72)$$

$$d\mathbf{f}_2 = \int_{\Omega} \mathbf{N}^T \left( \frac{\partial^2 F}{\partial \rho^2} - \eta \frac{\partial \tilde{g}}{\partial \rho} \right) d\boldsymbol{\rho} d\Omega + \gamma \int_{\Omega} \mathbf{B}^T \nabla d\boldsymbol{\rho} d\Omega - \eta \int_{\Omega} \mathbf{N}^T \mathbf{H} d\boldsymbol{\varepsilon} d\Omega - \int_{\Omega} \mathbf{N}^T d\boldsymbol{\mu} d\Omega \quad (3.73)$$

$$d\mathbf{f}_3 = \int_{\Omega} \mathbf{B}_m^T \tilde{f}' \mathbf{D}^0 \boldsymbol{\varepsilon} d\boldsymbol{\rho} d\Omega + \int_{\Omega} \mathbf{B}_m^T \mathbf{D} \mathbf{B}_m d\Omega d\mathbf{u} \quad (3.74)$$

where

$$\mathbf{H} = \frac{\partial \tilde{g}}{\partial \varepsilon_{ij}} \quad (3.75)$$

To simplify the notation the following definitions are introduced

$$d\mathbf{f}_1 = \mathbf{K}_{11} d\boldsymbol{\rho} + \mathbf{K}_{12} d\boldsymbol{\mu} \quad (3.76)$$

$$d\mathbf{f}_2 = \mathbf{K}_{21} d\boldsymbol{\rho} + \mathbf{K}_{22} d\boldsymbol{\mu} + \mathbf{K}_{23} d\mathbf{u} \quad (3.77)$$

$$d\mathbf{f}_3 = \mathbf{K}_{31} d\boldsymbol{\rho} + \mathbf{K}_{33} d\mathbf{u} \quad (3.78)$$

Which gives the following equation

$$\begin{pmatrix} \mathbf{K}_{11} & \mathbf{K}_{12} & \mathbf{0} \\ \mathbf{K}_{21} & \mathbf{K}_{22} & \mathbf{K}_{23} \\ \mathbf{K}_{31} & \mathbf{0} & \mathbf{K}_{33} \end{pmatrix} \begin{pmatrix} d\boldsymbol{\rho} \\ d\boldsymbol{\mu} \\ d\mathbf{u} \end{pmatrix} = - \begin{pmatrix} \mathbf{f}_1 \\ \mathbf{f}_2 \\ \mathbf{f}_3 \end{pmatrix} \quad (3.79)$$

where  $\mathbf{K}_{ij}$   $i = 1, 2, 3$   $j = 1, 2, 3$  are defined by:

$$\mathbf{K}_{11} = \int_{\Omega} \mathbf{N}^T \mathbf{N} d\Omega + \Delta t \int_{\Omega} \mathbf{B}^T \nabla \boldsymbol{\mu} \frac{\partial M}{\partial \rho} \mathbf{N} d\Omega \quad (3.80)$$

$$\mathbf{K}_{12} = \Delta t \int_{\Omega} \mathbf{B}^T M \mathbf{B} d\Omega \quad (3.81)$$

$$\mathbf{K}_{21} = \int_{\Omega} \mathbf{N}^T \left( \frac{\partial^2 F}{\partial \rho^2} - \eta \frac{\partial \tilde{g}}{\partial \rho} \right) \mathbf{N} d\Omega + \gamma \int_{\Omega} \mathbf{B}^T \mathbf{B} d\Omega \quad (3.82)$$

$$\mathbf{K}_{22} = - \int_{\Omega} \mathbf{N}^T \mathbf{N} d\Omega \quad (3.83)$$

$$\mathbf{K}_{23} = - \eta \int_{\Omega} \mathbf{N}^T \mathbf{H} \mathbf{B}_m^T d\Omega \quad (3.84)$$

$$\mathbf{K}_{31} = \int_{\Omega} \mathbf{B}_m^T \tilde{f}' \mathbf{D}^0 \boldsymbol{\varepsilon} \mathbf{N} d\Omega \quad (3.85)$$

$$\mathbf{K}_{33} = \int_{\Omega} \mathbf{B}_m^T \mathbf{D} \mathbf{B}_m d\Omega \quad (3.86)$$

As a next step in deriving the new method Newton-Raphson iterations will be implemented to prevent errors from accumulating at each time step.

### 3.1.6 Newton Raphson

Let  $\mathbf{R}(\mathbf{Y})$  denote the global residual at the current state  $\mathbf{Y}$  where

$$\mathbf{Y} = \begin{pmatrix} \rho \\ \mu \\ \mathbf{u} \end{pmatrix} \quad \mathbf{R}(\mathbf{Y}) = \begin{pmatrix} \mathbf{f}_1 \\ \mathbf{f}_2 \\ \mathbf{f}_3 \end{pmatrix} \approx \mathbf{0} \quad (3.87)$$

The goal is then to find a state  $\mathbf{Y}$  such that  $\mathbf{R}(\mathbf{Y}) \approx \mathbf{0}$ .

A Taylor expansion around a known residual  $\mathbf{R}(\mathbf{Y})$  gives

$$\mathbf{R}(\mathbf{Y}) = \mathbf{R}(\mathbf{0}) + \delta\mathbf{R}(\mathbf{Y}) + \dots = \mathbf{0} \quad (3.88)$$

where the dots indicate higher order terms and  $\delta\mathbf{R}(\mathbf{Y})$  is defined as

$$\delta\mathbf{R}(\mathbf{Y}) = -\frac{\partial\mathbf{R}}{\partial\mathbf{Y}}\delta\mathbf{Y} = -\mathbf{K}(\mathbf{Y})\delta\mathbf{Y} \quad (3.89)$$

Here

$$\mathbf{K}(\mathbf{Y}) = \frac{\partial\mathbf{R}}{\partial\mathbf{Y}} \quad (3.90)$$

defines the global stiffness matrix. Combining equations (3.88) and (3.89) results in

$$\delta\mathbf{Y} = \mathbf{K}^{-1}\mathbf{R}(\mathbf{Y}) \quad (3.91)$$

$$\mathbf{Y}^i = \mathbf{Y}^{i-1} + \delta\mathbf{Y}^i \quad (3.92)$$

where the  $i$  in (3.92) stands for the iteration index. This scheme will then be used repeatedly until a state  $\mathbf{Y}$  that satisfies  $\mathbf{R}(\mathbf{Y}) \approx \mathbf{0}$  is found.

### 3.1.7 Adaptive Mesh

In this section the local errors due to the space discretization will be reduced through a mesh refinement. The procedure of refining the mesh starts with an error estimation for each element, the errors are then compared to a given tolerance. For those elements with an error that do not satisfy the tolerance an adaptive scheme will be applied which will appear as a refinement of the space discretization.

#### Estimation of the local errors

In Section 3.1.4 two residuals  $\mathbf{f}_1$  and  $\mathbf{f}_2$  were derived from equations (3.30) and (3.32) which for completeness are stated again.

$$\frac{\partial \rho}{\partial t} - \Delta \mu = 0 \quad (3.93)$$

$$\frac{1}{\gamma} (F_{,\rho} - \mu - \gamma \rho_{,ii} - \eta \tilde{g}(\rho, \mathbf{u})) = 0 \quad (3.94)$$

where  $\Delta$  denotes the Laplacian which is defined by  $\Delta = \nabla \nabla$ . When deriving  $\mathbf{f}_1$  and  $\mathbf{f}_2$  approximations of the field variables  $\rho$ ,  $\mu$  and  $\mathbf{u}$  were made. Inserting these approximations into equations (3.93) and (3.94) introduces an error to the equations. When calculating the residuals these errors are compensated by the multiplication of the weight functions and integration over the domain  $\Omega$  cf.[6]. These errors will however still influence the solution on local level for each element  $e$ . The error estimated for element  $e$  is denoted  $R_e^i$  and calculated as the residual that comes from inserting the approximations of the field variables directly into equations (3.93) and (3.94).

For example would  $R_e^1$  define the residual that comes from inserting the approximations into equation (3.93) i.e.

$$R_e^1 = \mathbf{N} \frac{(\rho - \rho_n)}{\Delta t} |_e \quad (3.95)$$

Where use have been made of

$$\dot{\rho}_e \approx \frac{\rho - \rho_n}{\Delta t} \quad (3.96)$$

$$\nabla \nabla = \Delta \quad (3.97)$$

$$\Delta \mathbf{N} \boldsymbol{\mu} = \nabla \mathbf{B} \boldsymbol{\mu} \quad (3.98)$$

$$\nabla \mathbf{B} = 0 \quad (3.99)$$

and  $|_e$  means that the field variable is calculated in element  $e$ .

When estimating the local error in the space discretization the residual  $R_e^i$  does not constitute the whole error. The error is also influenced by the difference in the field variables between two neighboring element. This contribution to the local error is for two elements connected trough  $\tau$  defined as

$$J_\tau^2(t) = (\mathbf{B}\boldsymbol{\rho}|_{e_1} - \mathbf{B}\boldsymbol{\rho}|_{e_2})^T \mathbf{n}_1 \quad (3.100)$$

$$J_\tau^1(t) = (\mathbf{B}\boldsymbol{\mu}|_{e_1} - \mathbf{B}\boldsymbol{\mu}|_{e_2})^T \mathbf{n}_1 \quad (3.101)$$

$$(3.102)$$

where  $\tau$  denotes the sides of element  $e$  and with the exception that if the current element has one ore more side  $\tau$  connected to the outer boundary the following definition will be used instead.

$$J_\tau^2(t) = 2(\mathbf{B}\boldsymbol{\rho}|_e)^T \mathbf{n} \quad (3.103)$$

$$J_\tau^1(t) = 2(\mathbf{B}\boldsymbol{\mu}|_e)^T \mathbf{n} \quad (3.104)$$

$$(3.105)$$

Here  $\mathbf{n}_1$  denotes the unit normal vector to  $\tau$  pointing from element  $e_1$  to element  $e_2$  and  $\mathbf{n}$  denotes the unit normal vector to  $\tau$  pointing away from the body  $\Omega$ .

The local error estimators  $\eta_e^1(t)$  and  $\eta_e^2(t)$  are for each element defined as

$$\eta_e^j(t) = h_e \|R_e^j\|_{L^2(e)} + \sum_{\tau \in \partial e} \left(\frac{1}{2} h_\tau \|J_\tau^j\|_{L^2(\tau)}^2\right)^{1/2}, \quad j = 1, 2. \quad (3.106)$$

where  $h_e$  denotes the element area,  $h_\tau$  denotes the length of  $\tau$  and  $\|X\|_{L^2(e)}$  is defined as.

$$\|X\|_{L^2(e)} = \left(\int_{h_e} X^T X dh_e\right)^{1/2}. \quad (3.107)$$

Finally the local error is estimated as

$$\eta_e(t) = \left((\eta_e^1(t))^2 + \frac{1}{\gamma^2} (\eta_e^2(t))^2\right)^{1/2} \quad (3.108)$$

## Re-meshing

After  $\eta_e(t)$  has been calculated for each element they are compared to a the tolerance LET "local error tolerance" and depending on the results of these comparisons the following decisions are made

- if  $\eta_e(t) > LET$  split the element into two new elements, (this procedure is called refinement)
- if  $\eta_e(t) < LET/\sqrt{3}$  coarsen the element

If an element is about to be refined this is done by inserting a new node on the longest side  $\tau$  of the element and draw a line between this node and the node opposite the longest side. The refinement process is sketched in Figure 3.5.

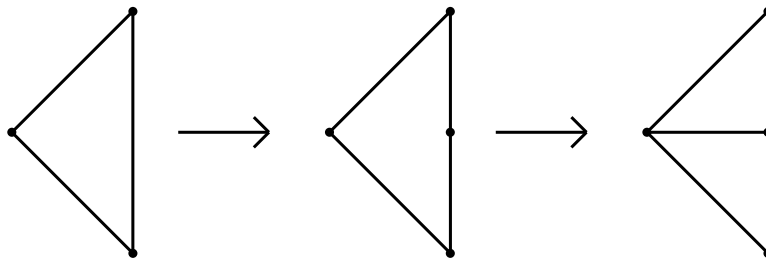


Figure 3.5: Illustration of the splitting process

If the longest side is connected to another element this element has to be split as well since no element should contain a *loose node*. Sometimes the neighboring element has not been refined as many times as the element that is supposed to be refined and in these cases the neighboring element has to be refined before the new node is added. For better understanding of this procedure Figure 3.6- 3.9 are shown.

Imagine that element 10 in the mesh shown in Figure 3.6 is supposed to be refined. Since splitting element 10 leaves element 9 with a *loose node*

element 9 has to be split as well cf. Figure 3.7. Now imagine that the new element 19 needs to be refined. Splitting element 19 would leave element 11

with a *loose node* but since element 11 has not been refined as many times as element 19 a problem occurs. To resolve this problem element 11 must be refined before the new node is inserted

After element 11 has been refined the last *loose node* can be connected in a correct way cf. Figure 3.9.

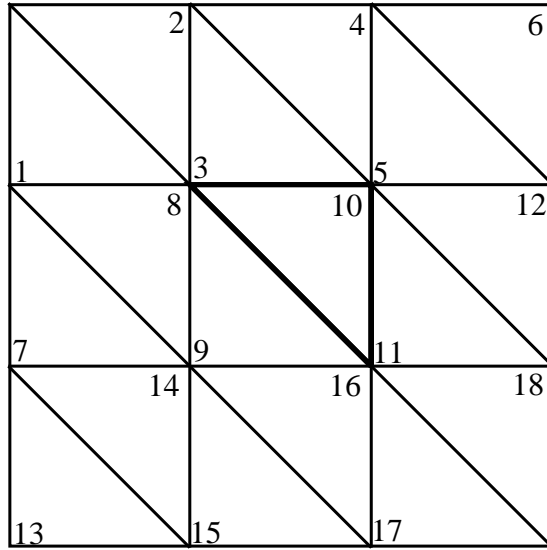


Figure 3.6: Original mesh

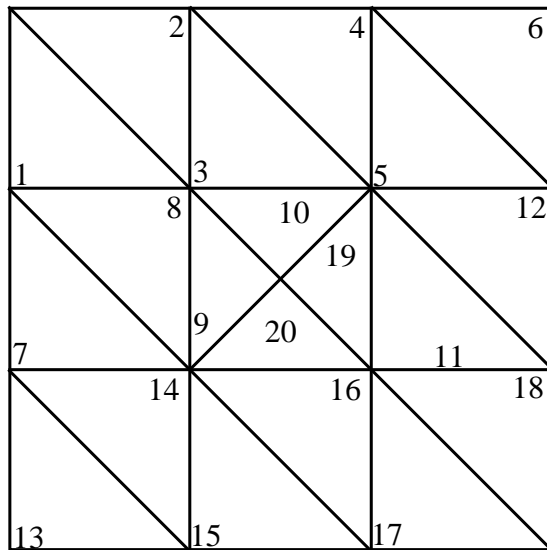


Figure 3.7: Original mesh refined one time

If an element is about to be coarsened the line  $\tau$  that was inserted during a previous refinement is supposed to be removed. However this  $\tau$  can not be removed before checking if all the neighboring elements that share the same nodes as  $\tau$  also are about to be coarsened. If any of these neighboring

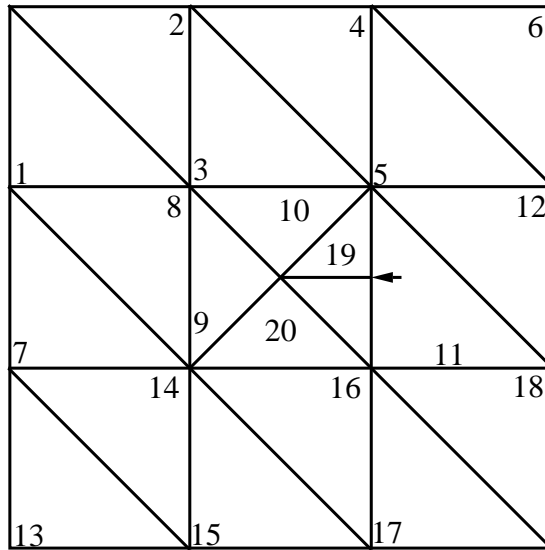


Figure 3.8: Displaying the *loose node*

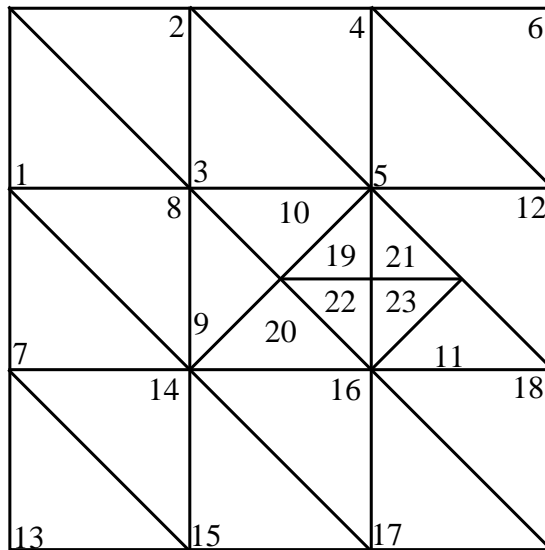


Figure 3.9:

elements is not set to be coarsened the element in question have to stay untouched during this re-meshing.

### 3.1.8 Results from Part B

To demonstrate the presented scheme the procedure is applied to **Example 1**, cf. 1.1.1. The structure considered consists of a cantilever beam loaded with a point load  $F$ , cf. Fig.3.10a. The initial material distribution is shown in Figure.3.10b.

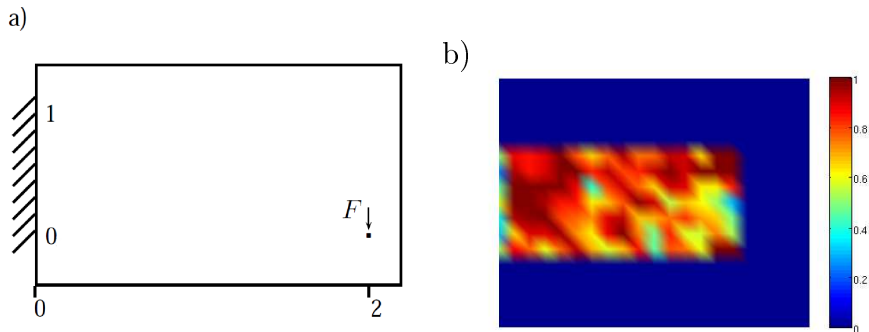


Figure 3.10: a) Illustration of the design space, b) Initial material distribution

The initial spatial discretization is constructed with 442 triangular elements and is illustrated in Figure 3.11

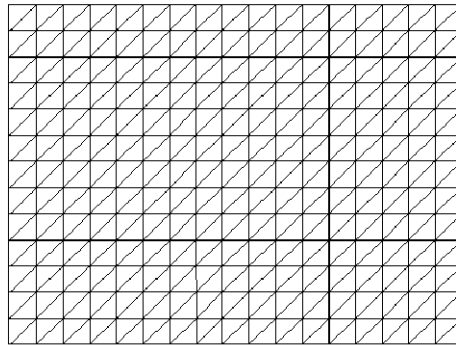


Figure 3.11: Initial spatial discretization

#### The effect of changing $\gamma$

The optimized density distribution for  $\gamma = 6 \cdot 10^{-4}/m^2$  is shown in Figure 3.12a, for  $\gamma = 2 \cdot 10^{-4}/m^2$  in Figure 3.12b and for  $\gamma = 4 \cdot 10^{-5}/m^2$  in

Figure 3.12c. From these figures it is confirmed that the density distributions come close to  $\rho \in \{0, 1\}$  with the exception of the thin interfaces between regions where  $\rho = 1$  and  $\rho = 0$ . A minor deviation from  $\rho \in \{0, 1\}$  can also be seen in the point where the load is applied, here the density is slightly above 1. When comparing the optimized structures illustrated in Figure 3.12a,b and c the effect of changing  $\gamma$  becomes clear i.e a smaller  $\gamma$  returns thinner interfaces. The effect of changing  $\gamma$  is also seen in that a smaller  $\gamma$  allow more regions of interfaces which in Figure 3.12a,b and c appears as a smaller  $\gamma$  returns a structure with more holes in it.

### Mesh

In the space discretization performed in this thesis focus were put on resolving the interface. For this reason all the parts except from  $J_\gamma^2$  are neglected in the error estimation cf. 3.1.7. In Figure.3.13a,b,c the space discretization after optimization for each  $\gamma$  are illustrated. Since some data can be hard to read from these figures **Table I** containing additional data for each mesh is also included.

**Table I**

$\gamma /m^2$	Total number of elements	Number of elements used to resolve the interface
$6 \cdot 10^{-4}$	18178	17
$2 \cdot 10^{-4}$	61215	17
$4 \cdot 10^{-5}$	251793	21

Table I: Data from space discretization shown in Figure 3.13

Since the interface is hard to define the number of elements used to resolve these are only approximate numbers.

According to **Table I** roughly the same number of elements are used to resolve the interfaces for different  $\gamma$  but the total number of elements used in each space discretization differs widely. This is partly an effect of that a smaller  $\gamma$  allow more gradients but also an effect of that the interface of a smaller gamma is resolved with smaller elements which results in that more elements are needed to connect these *interface elements* with the rest of the elements. From these figures one clearly sees the importance of using an adaptive space discretization.

### Illustration of the optimization path

In Figure 3.14 the process of optimizing the structure shown in Figure 3.10b is illustrated. This optimization is performed using  $\gamma = 2 \cdot 10^{-4}/m^2$  and in the figure every 50th step is shown.

### Discussion of $\mu$

Figure 3.15 are included to show that, for all three  $\gamma$ , the solutions converged to a state where  $\mu$  is constant over the whole domain. This is a property of the method that was derived in Section 3.1.2 and also used as a check to terminate the simulations.

### Effect of changing LET "local error tolerance"

In Figure 3.16 two optimization simulations are performed on the same structure using the same  $\gamma = 6 \cdot 10^{-4}/m^2$ . What differs these two simulations is that they are run with two different local error tolerances  $LET$  (cf. Section 3.1.7). The difference in  $LET$  will appear as a change in the space discretization and the two simulations are compared to emphasize that the mesh dependency is no longer present.

In Figure 3.16 it is shown that the two simulations run with different  $LET$  returns basically the same structure. The number of elements needed for the space discretization of the optimized structures are presented in the **Table II**.

**Table II**

$LET$	Total number of elements	Number of elements used to resolve the interface
$2 \cdot 10^{-2}$	18178	33
$4 \cdot 10^{-3}$	73834	80

### Energies

Commenting on the evolution of the energies in functional  $E$  (cf. Section 3.1) is difficult since the functional depends on the spatial discretization. In Figure 3.17a the first two seconds of a simulation performed with  $\gamma = 4 \cdot 10^{-5}/m^2$  is shown, in this figure a "jump" in the energies can be observed. This "jump", is the result of a changed space discretization. From Figure 3.17a it is clear that the total energy is decreasing for each space discretization. Comparing

Figure 3.17b with Figure 3.14 the same phenomena is observed, namely that the main changes in the structure occurs in the beginning of the optimization. The energies that are shown in Figure 3.17 are defined by equations (1.26) , (3.2) , (3.3) and (3.4) which state that

$$w = \frac{1}{2}\varepsilon_{ij}D_{ijkl}\varepsilon_{kl} \quad (3.109)$$

$$F(\rho_e) = (\rho_e^2(1 - \rho_e)^2 e^{15(0.5 - \rho_e)^2} + \rho_e^2(1 - \rho_e)^2 10) \quad (3.110)$$

$$S(\boldsymbol{\rho}) = \int_{\Omega} \rho_{e,i}\rho_{e,i}d\Omega \quad (3.111)$$

$$E(\boldsymbol{\rho}, \boldsymbol{\rho}_{,i}, \mathbf{u}) = \int_{\Omega} (F(\rho_e) + \frac{\gamma}{2}\rho_{e,i}\rho_{e,i})d\Omega + \eta \int_A w(\rho_e, \epsilon_{ij})d\Omega \quad (3.112)$$

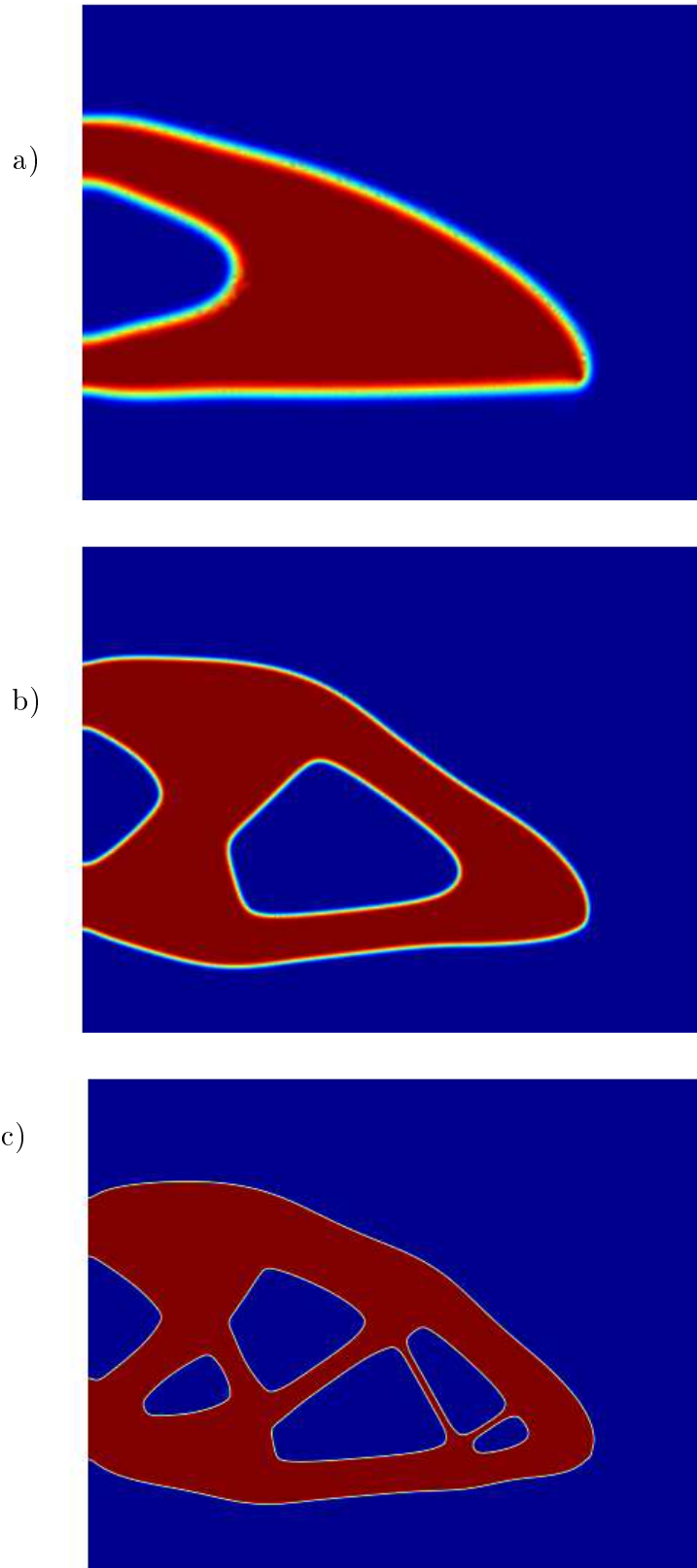


Figure 3.12: Optimized structures for a)  $\gamma = 6 \cdot 10^{-4}/m^2$  b)  $\gamma = 2 \cdot 10^{-4}/m^2$   
 c)  $\gamma = 4 \cdot 10^{-5}/m^2$

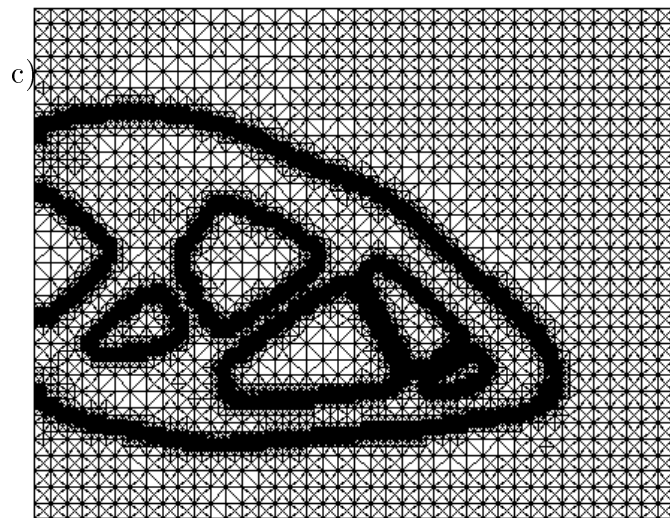
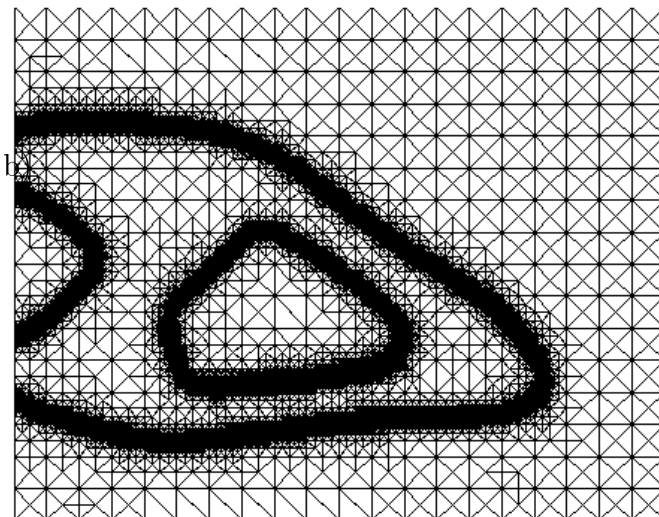
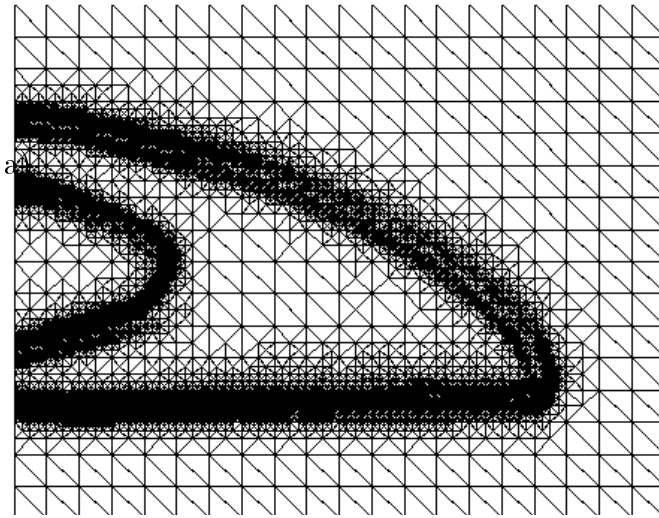


Figure 3.13: Final space discretization for a)  $\gamma = 6 \cdot 10^{-4}/m^2$  b)  $\gamma = 2 \cdot 10^{-4}/m^2$  c)  $\gamma = 4 \cdot 10^{-5}/m^2$

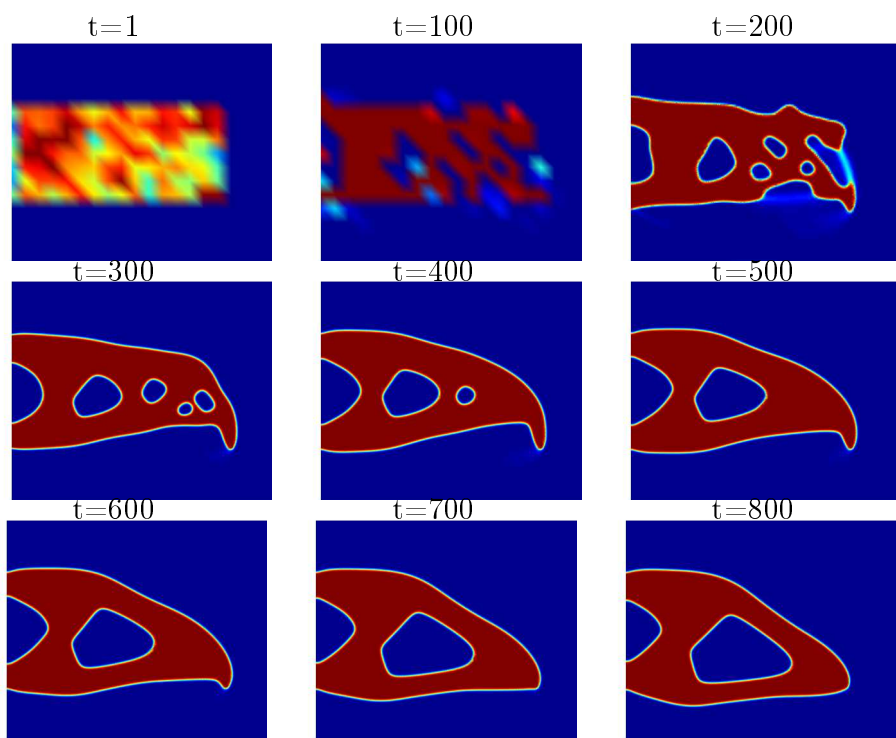


Figure 3.14: Illustration of the optimization process

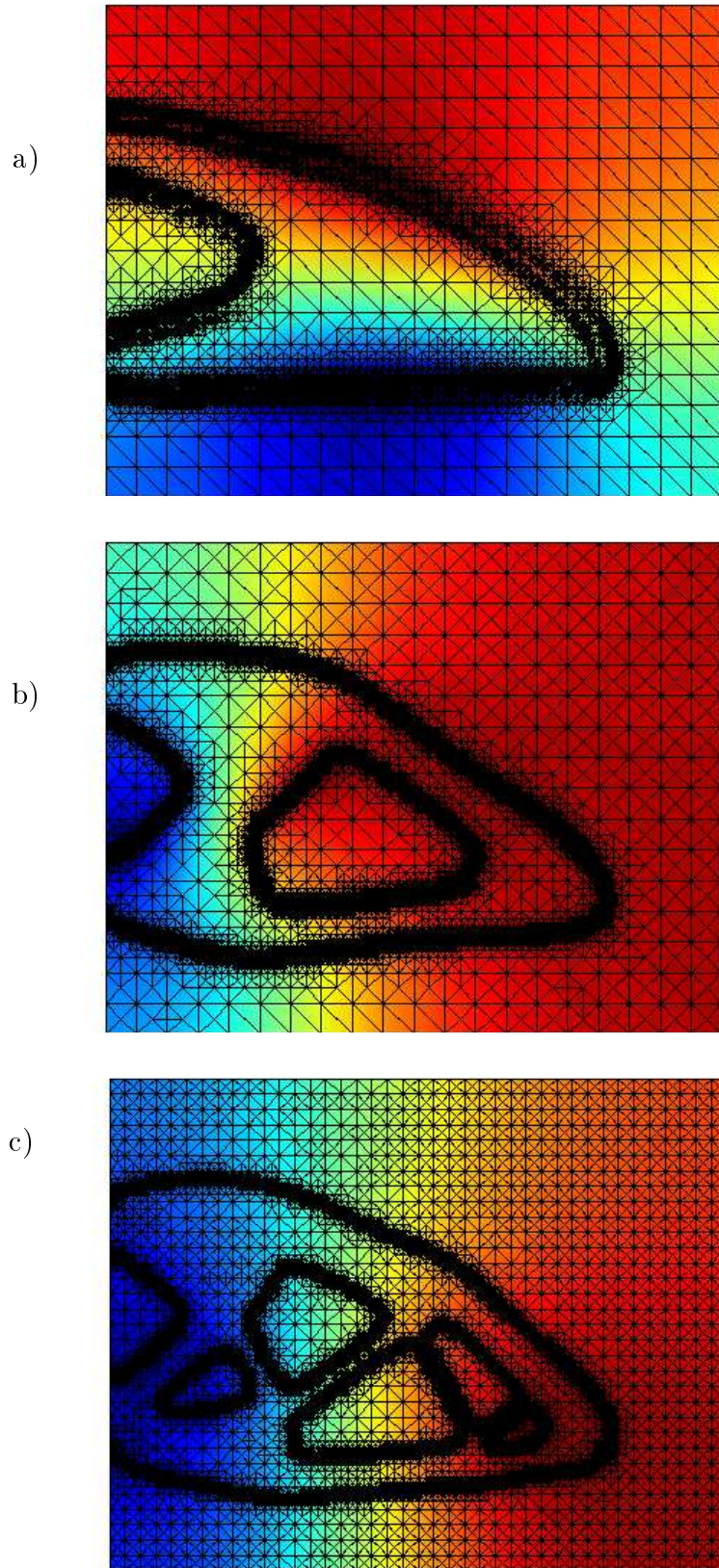


Figure 3.15: Distribution of  $\mu$  for a)  $\gamma_{33} = 6 \cdot 10^{-4}/m^2$  b)  $\gamma = 2 \cdot 10^{-4}/m^2$  c)  $\gamma = 4 \cdot 10^{-5}/m^2$

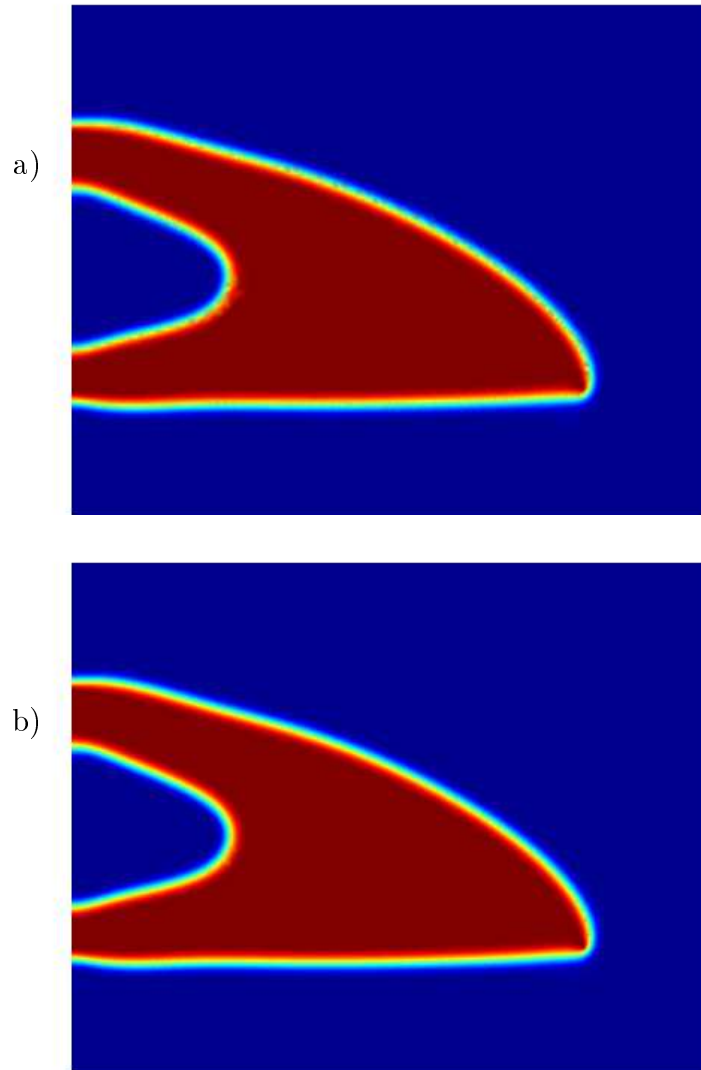


Figure 3.16: Optimized structures for  $\gamma = 6 \cdot 10^{-4}/m^2$  and a)  $LET = 2 \cdot 10^{-2}$   
b)  $LET = 4 \cdot 10^{-3}$

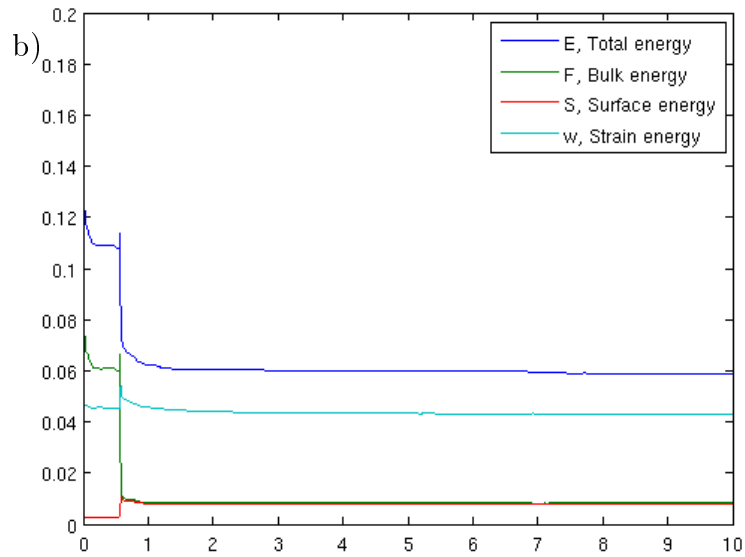
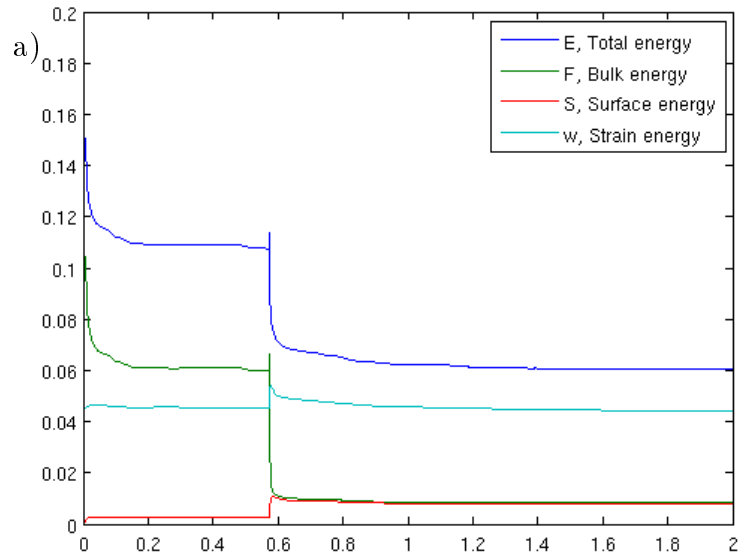


Figure 3.17: a)Energy history after 2 seconds b)Energy history after 10 seconds

## 3.2 Appendix1

### 3.2.1 The matrices in equations (1.11) - (1.13)

$$\mathbf{t} = \begin{pmatrix} t_x \\ t_y \end{pmatrix} \quad \mathbf{b} = \begin{pmatrix} b_x \\ b_y \end{pmatrix} \quad (3.113)$$

$$\mathbf{N}_m = \begin{pmatrix} N_1 & 0 & N_2 & 0 & N_3 & 0 \\ 0 & N_1 & 0 & N_2 & 0 & N_3 \end{pmatrix} \quad (3.114)$$

$$\mathbf{B}_m = \tilde{\nabla}^T \mathbf{N}_m = \begin{pmatrix} \frac{\partial N_1}{\partial x} & 0 & \frac{\partial N_2}{\partial x} & 0 & \frac{\partial N_3}{\partial x} & 0 \\ 0 & \frac{\partial N_1}{\partial y} & 0 & \frac{\partial N_2}{\partial y} & 0 & \frac{\partial N_3}{\partial y} \\ \frac{\partial N_1}{\partial y} & \frac{\partial N_1}{\partial x} & \frac{\partial N_2}{\partial y} & \frac{\partial N_2}{\partial x} & \frac{\partial N_3}{\partial y} & \frac{\partial N_3}{\partial x} \end{pmatrix} \quad (3.115)$$

$$\tilde{\nabla} = \begin{pmatrix} \frac{\partial}{\partial x} & 0 \\ 0 & \frac{\partial}{\partial y} \\ \frac{\partial}{\partial y} & \frac{\partial}{\partial x} \end{pmatrix} \quad (3.116)$$

### 3.2.2 Derivatives of $\tilde{f}_i$

The derivatives of  $\tilde{f}_i$  are calculated as

$$(\tilde{f}_3)'_{\rho} = \frac{a(2\rho k e^{-2k\rho} + b + e^{-2k\rho})}{(b + e^{-2k\rho})^2} \quad (3.117)$$

$$(\tilde{f}_3)''_{\rho} = - \frac{4ake^{-2k\rho}(k\rho b - \rho k e^{-2k\rho} - b - e^{-2k\rho})}{(b + e^{-2k\rho})^3} \quad (3.118)$$

where the derivatives of  $\tilde{f}_1$  and  $\tilde{f}_2$  are considered trivial and for that reason not written down.

### 3.2.3 Derivatives of $\tilde{g}$

$$\begin{aligned} \frac{\partial \tilde{g}}{\partial \rho} &= (\tilde{f}_3)''_{\rho} \varepsilon_{ij} D_{ijkl} \varepsilon_{kl} \\ \frac{\partial^2 \tilde{g}}{\partial \rho^2} &= (\tilde{f}_3)'''_{\rho} \varepsilon_{ij} D_{ijkl} \varepsilon_{kl} \\ \frac{\partial \tilde{g}}{\partial \varepsilon_{ij}} &= 2(\tilde{f}_3)'_{\rho} D_{ijkl}^0 \varepsilon_{kl} = \frac{2(\tilde{f}_3)'_{\rho}}{\tilde{f}_3} \sigma_{ij} \end{aligned}$$

# Bibliography

- [1] Peter W. Christensen and Anders Klarbring: *An Introduction to Structural Optimization* 2009
- [2] O.C.Zienkiewicz and R.L.Taylor: *The Finite Element Method* FOURTH EDITION Vol.1 Basic Formulation and Linear Problems 1994
- [3] O.C.Zienkiewicz and R.H.gallagher: *Numerical Methods in Engineering* Vol.7,No.3, 1973
- [4] Jos'e Figueroa-O'farrill: *Brief Notes On The Calculus Of Variations*
- [5] Jim Fischer: *Introduction To The Calculus Of Variations* March 20,1999
- [6] Niels Ottosen and Hans Petersson: *Introduction to the FINITE ELEMENT METHOD* 1992
- [7] Lars-Christer Böiers: *LECTURES ON OPTIMISATION* 2007